EFFECTS OF CONSOLIDATION PARAMETERS ON CREEP, FATIGUE AND DYNAMIC MECHANICAL BEHAVIOUR OF SELF-REINFORCED POLYPROPYLENE COMPOSITES

By

Wanyama, Paul Simiyu

B. Ed. Sc. (Hons)

A Thesis Submitted in Partial Fulfillment of the Requirements for the Award of the Degree of Master of Science in the School of Pure and Applied Sciences of Kenyatta University

March 2014

DECLARATION

I declare that the work presented in this thesis is my original work and has not been presented for the award of any degree or any other award in any University

All sources of information have particularly been acknowledged by means of references.

Wanyama, Paul Simiyu Signature Date

Department Of Physics

Kenyatta University ...…….. ……

P.O.BOX 43844-00100

NAIROBI-KENYA

We confirm that the work reported in this thesis was carried out by the candidate under our supervision.

Dr. C. M. Migwi Signature Date

Department Of Physics

Kenyatta University ...…….. ……

P.O.BOX 43844-00100

NAIROBI-KENYA

Dr. D. B. BEM Signature Date

Department Of Physics

Kenyatta University ...…….. ……

P.O.BOX 43844-00100

NAIROBI-KENYA

DEDICATION

This thesis is dedicated to my beloved parents, my wife: Beatrice, my daughter: Lovien, my sons: Cleverence and Espen.

ACKNOWLEDGEMENTS

Firstly, I give thanks and honour to The Almighty God through whom everything is possible. The completion of this work has also been the consequence of voluntary investment of time and mental resources by many dedicated people.

I would like to say a special thank you to my supervisors Dr. C.M. Migwi and, Dr. D.B. Bem for their willingness to assist me with the valuable scientific ideas, critique and encouragement necessary to undertake this work. In particular, I acknowledge the compassionate treatment accorded by Dr. C.M. Migwi especially during challenging moments. I would like to express my thanks and sincere gratitude to Dr. D. B. Bem for earnestly accepting to team up with Dr. C.M. Migwi, to lead me through this research. It is impossible to thank these gentlemen enough in a few paragraphs.

I am profoundly grateful to the entire Department of Physics Kenyatta University for the amble time I have had during the entire period of study. I would also like to thank all those who work in the physics laboratory, Department of Physics Kenyatta University where most of these work was done. I appreciate the hard work, creativity and determination of Dr. A. S Merenga for working tirelessly to ensure the DMA equipment I used for data collection was in good operating mode. Thanks to my colleagues for their support and encouragement. Finally, I would like to thank my family for all their support throughout my entire study time. They helped me through tough decisions and supported me when I needed help. They are a large part of my success and without them this wouldn't have been possible. Lastly but not least, I ascribe all the praise and honour to the Almighty God for His grace.

TABLE OF CONTENTS

ABBREVIATIONS, AND ACRONYMS

ASTM	American society for testing and materials
BF	Basalt fiber
DMA	Dynamic mechanical analysis
DSC	Differential Scanning Calorimetry
DTG	Differential thermogravimetry
DR_1	Draw ratio 1
DR_2	Draw ratio 2
DR_3	Draw ratio 3
ELV	End- of-life of vehicles
EPE	Ethylene propylene elastomer
F_{w1}	Fiber weight fraction 1
F_{w2}	Fiber weight fraction 2
F_{w3}	Fiber weight fraction 3
GF	Glass fiber
GFRPPCs	Glass fiber reinforced polypropylene composites
HDPE	High density polyethylene
IFWI	Instrument Falling Impact test
NF	Natural fiber
PP	Polypropylene
SRPPCs	Self-reinforced polypropylene composites
SRPCs	Self-reinforced polymer composites
t_1	Consolidation time 1
t_2	Consolidation time 2
t_3	Consolidation time 3
TGA	Thermogravimetric analysis
Tc_1	Consolidation temperature 1

Tc_2	Consolidation temperature 2
Tc_3	Consolidation temperature 3
WLF	William- Landel-Ferry

SYMBOLS

A	Amplitude ratio
A	Frequency factor
$E_{app.}$	Apparent activation energy decomposition,
T_a	Absolute temperature.
r	Heating rate
a_T	Shift factor
C	Concentration
C_1 and C_2	Constants in the WLF equation
D	Cumulative damage
E	residual modulus
E_o	Initial modulus
E*	Complex modulus
E’	Storage modulus
E”	Loss modulus
ΔEa	Activation energy
J	Creep compliance
k	Boltzmann’s constant
M	The actual mass of the sample
M_o	The initial mass of the sample
M_f	The final mass of the sample
N	Number of cycles
n	Exponent of t in Findley model
n_1	Exponent for the cumulative damage (D) in the cumulative damage equation at the beginning of fatigue life cycles
n_2	Exponent for the cumulative damage (D) in the cumulative damage equation at the end of fatigue life cycles
R	Stress ratio
R	Universal gas constant

t	time
$\dot{t}$	Shifted (reduced time)
T	Temperature
T	Experimental temperature
T_o	Reference temperature (T_{ref})
T_m	Melting point
T_g	Glass transition temperature
E_a	Activation energy
χ_1	Material constant, in the cumulative damage equation at the beginning of fatigue life cycles
χ_2	Material constant in the cumulative damage equation at the end of fatigue life cycles
δ	Phase lag
ε	Total strain
ε_o	Instantaneous strain after application of stress
ε_c	time-dependent strain
ε_B	Total strain (Burger)
$\dot{\varepsilon}_B$	Creep rate for Burgers model
ε_F	Total strain (Findley)
$\dot{\varepsilon}_F$	Creep rate for Findley model
ε_{M1}	Strains of the Maxwell spring
ε_{M2}	Strain of Maxwell dashpot
ε_K	Strain of Kelvin unit
E_M	Modulus of the Maxwell spring
η_M	Viscosity of the Maxwell dashpot
E_K	Modulus of the Kelvin spring
η_K	Viscosity of the Kelvin dashpot

σ_o	Initially applied stress
α	Mass conversion rate during thermal decomposition
β	Reaction order
σ	Stress
σ_{min}	Minimum stress
σ_{max}	Maximum stress
ω	Angular frequency

LIST OF FIGURES

LIST OF TABLES

ABSTRACT

Environmental concerns, production costs, reprocessability, and weight of traditional polymer-based composites are major issues that have heightened research in the field of materials science. Thus research on the development of new classes of composites called self-reinforced polymer composites has intensified. Self-reinforced polypropylene composites prepared by compression moulding were examined in this study. This study produced composites (SRPPCs) reinforced with polypropylene fibers of different draw ratios (Dr: 11, 8, 5, 2) and different fiber weight fractions (Fw; 15, 12, 9, 6 and 3). Composites were fabricated at consolidation temperatures in the range 163 to 175^{o}C, and consolidation time in the range 30 to 130 seconds. This study investigated the effects of consolidation temperature, consolidation time, fiber draw ratio and fiber weight fraction on dynamic mechanical properties, fatigue behaviour, creep deformation and thermal stability of SRPPCs. The samples were subjected to dynamic mechanical analysis (DMA) in the temperature range 30 to 110^{o}C at frequency of 1Hz. From the DMA results, it was observed that storage modulus was greatest at optimum consolidation temperature of 170^{o}C, stiffness increased with consolidation time, fiber draw ratio and fiber weight fraction. Fatigue test was also performed on the samples at constant cyclic strain amplitude of 20μm, frequency of 5Hz, and temperature 35^{o}C. Fatigue resistance and fatigue endurance was improved significantly at consolidation temperature of 170^{o}C, consolidation time of 130 seconds, fiber draw ratio of 11, and fiber weight fraction of 15wt%. Short-term isothermal creep tests were carried out at different temperatures ranging from 30 to 90^{o}C under an applied stress of 5MPa. Remarkable improvement on creep resistance occurred when consolidation temperature, consolidation time, fiber draw ratio and fiber weight fraction were maintained at 170 ^{o}C, 130 seconds, 11 and 15wt% respectively. Burgers and Findley power law models could satisfactorily be applied to analyse the short-term creep behaviour of the composites as well as predict the creep deformation beyond the experimental time of 12 minutes. Creep master curves were created using time-temperature superposition principle (TTSP). Using the master curves, creep deformation of order 10^{8} minutes could be predicted. The temperature dependence of the shift factors could best be described by the Arrhenius equation. All these positive gains made in mechanical properties are attributed to fiber drawing which enhances molecular orientation (crystalline regions) and minimizes segmental movement of the chain molecules. Thermal decomposition tests on the samples exhibited improved thermal stability of the self-reinforced polypropylene composites.

CHAPTER ONE

INTRODUCTION

1.1 Background to the Study

Nowadays considerable efforts are being made to develop composite materials to provide solutions to a variety of challenges. Among them four issues require urgent attention. The new environmental challenges, reducing the energy needed to create and process materials, reducing the volume and weight of materials needed and benefitting from the improved performance they offer are all major topics in the field of polymer research (Gurarslan *et al*., 2011: Stella, 2013).

The demand for light weight and high performance materials in industries such as aerospace, automotive, construction, electronics and many others has led to increase in use of polymer composites and particularly thermoplastic composites (Cabrera, 2004; Gurarslan *et al*., 2011: Stella, 2013). This trend is due to polymer composites offering high performance materials with minimal weight when compared with traditional materials such as high strength steels. This increased usage brings with it an increased focus on the environmental impact of these materials. In particular, the ability to recycle materials at the end of component life is a very important factor in materials selection.

The negative environmental impact of the steadily increasing use of plastic and composite materials requires the development of new combinations of materials, possibly with improved properties, but with reduced environmental harm.

Consequently, the development of recycling friendly thermoplastic composites has become a top priority. In fact, there is a growing interest to either improve the methods for recycling and reusing existing composites, or develop new and intrinsically more suitable composites (Chen *et al*., 2010; Gurarslan *et al*., 2011: Stella, 2013).

The need to improve the recyclability (via reprocessing) of polymeric materials including thermoplastic and thermoplastic composites has become a key issue recently. This aim is even supported by the European Union directive on the end-of-life of vehicles (ELV). This directive states that no later than 2015 the reuse and recovery of all vehicles shall be increased to a minimum of 95% and recycling shall be increased up to 85% by an average weight per vehicle (Directive 2000/53/EC, András *et al*., 2009).

Isotactic homopolymer polypropylene (PP) is one of the most versatile of the bulk of polymers due to a combination of good mechanical and chemical properties, re-processability, as well as low cost. Hence PP has secured its position in a wide range of consumer and industrial products, manufactured by several high-volume forming methods (www.polymers.com). Injection molded PP, the largest of the PP grade, can be used in electronic and electrical appliances, house wares, bottle caps, and toys. Film grade PP can be found in the packaging of sweets and cigarettes, tapes, labels and electronic films. PP fibers are used in carpets, clothing, ropes and strings (DeWitt 35th, Annual World Petrochemical Conference, 2010).

Considerable efforts have been devoted to develop more environment friendly engineering materials with superior properties. This has led to the development of a new class of composites called self-reinforced polymer composites (Pegoretti, 2007; Matabola *et al*., 2009; Kmetty *et al*., 2010), in which both reinforcement and matrix are from the same polymer family. Self-reinforced polymer composites offer a range of advantages over the traditional fiber reinforced composites such as GFRPCs. First is the advantage of recyclability. As SRPCs composites are 100% thermoplastic, their recyclability is a very simple process. Unlike more traditional fiber reinforced composites, Self-reinforced polymer composites do not require the reinforcement to be separated from the matrix before effective recycling can take place (Hine *et al*., 2003; Houshyar *et al*., 2003; Houshyar *et al*., 2006; Alcock *et al*., 2006; Bárány *et al*., 2006; Alcock *et al*., 2007; Bhattacharyya *et al*., 2009; Bárány *et al*., 2009). At the end of the product life, a component can simply be re-melted and re-granulated. These granules can then be reprocessed into new components. This enhanced recyclability is desirable to satisfy the new environmental legislation which is currently targeting high volume industries particularly the automotive industry (Directive 2000/53/EC).

Secondly, self-reinforced polymer composites are reinforced with the same low density polymer from which the matrix is made. This means that although a significant increase in properties is gained, there is no increase in the density of the material. Hence, extremely light weight materials can be fabricated and so very significant weight loss on finished components can be achieved (Morgan *et al*., 2009). Because the reinforcement and the matrix are compatible chemically, fiber-matrix adhesion is not an issue. Fiber manufactured from the same polymer with the

matrix provides adequate reinforcing strength, resulting in a self-reinforced polymeric composite material with improved specific stiffness, and specific strength. Additionally, the need for coupling agents is completely eliminated, and the waste/scrap materials can be recycled by melting which satisfies the demand for green materials.

Another benefit of self-reinforced polymer composites is increased strength. Self-reinforced polymer composites offer significantly better properties than the virgin polymers from which they are made. For example Cabrera *et al*., (2004), have shown that at room temperature self-reinforced polypropylene composites display a modulus of 5.9 GPa, which is significantly above that of the unmodified PP (around 1.1 GPa). This has a very significant positive contribution towards achieving the desire for high strength lightweight materials. From the tooling and handling standpoint, the self-reinforced PP composites are also better than the glass fiber reinforced materials. Tool life is improved because the SRPPC is nonabrasive, and the processor does not encounter the handling issues associated with glass fibers. Because of the lower pressure required to process the self-reinforced composite, thermoforming is a very attractive processing alternative. This reduces capital costs (Loos *et al*., 2001; Ward *et al*., 2004; Abdullah *et al*., 2005; Alcock *et al*., 2006; Mckownm *et al*., 2007; Alcock *et al*., 2007).

Although self-reinforced polymer composites have many significant advantages they are not without their disadvantages. The main disadvantage is the temperature sensitivity. During processing, temperature must be controlled accurately in order to

melt only the matrix material while keeping the reinforcement undamaged by the heat. This leads to relatively small processing windows for these materials and consequently they can be difficult to process (Hine *et al*., 2003).

Successful production of SRP composites is based on the establishment of a suitable processing window whereby proper fiber/matrix adhesion is achieved without compromising the fiber properties (Houshyar *et al*., 2005; Barany *et al*., 2006; Alock *et al*., 2006; Alock *et al*., 2007; Barkoula, 2008; Alock *et al*., 2008). Various fabrication methods can produce self-reinforced polymer composites. One such method is film stacking (Matabola *et al*., 2009; Kmetty *et al*., 2010). This method is favored because it offers a wide processing window (up to about 40^{o}C), freedom of material selection and does not involve expensive pre-production processes (Houshyar *et al*., 2004; 2005).

The mechanical properties of self-reinforced polymer composites are dependent on microstructure and thermo-mechanical history (Peterlin, 1975; Samuels, 1985). The fabrication of these composites requires heating, but highly oriented polymer structures experience shrinkage forces in the drawn direction upon heating due to thermal energy allowing relaxation to higher entropy (De Candia *et al*., 1985; Trznadel *et al*., 1985; Bastiaansen *et al*., 1989). Thus there is always a risk that shrinkage and relaxation may occur during composite consolidation. If complete relaxation is allowed to occur, then the high tensile properties achieved during the fiber/tape drawing process will be reduced, hence negatively affecting the resulting composite. In order to limit or prevent this relaxation, it is important to carefully

define and control the parameters used to consolidate the composite into a load bearing structure. Within the processing window, mechanical properties are expected to vary as the micro-structural mechanisms of shrinkage and lateral flow compete. By creating a range of composite specimens with fibers of various draw ratios and different fiber weight fractions over a range of processing temperatures and times, the effect on mechanical properties can be established. The aim of this study was to investigate the dynamic mechanical properties, creep behavior, fatigue response and thermal stability of self-reinforced polypropylene composites fabricated using polypropylene fibers of various draw ratios as a function of consolidation temperature, consolidation time, fiber draw ratio and fiber weight fraction.

1.2 Statement of the research problem

Increased demand for materials that are environment friendly, require less energy to process, are light weight, have high specific strength and stiffness and are easily recycled has led to the high desire for an in-depth understanding of self-reinforced polymer composites. Self-reinforced polymer composites have good qualities. However, the quality of mechanical properties of SRPCs is determined by the accurate control of consolidation parameters and the properties of the reinforcement. If not well catered for, the effects of these conditions could impact negatively on the applications of SRPCs. In order to tailor these materials to desired application areas, the effects of fabrication conditions and the characteristics of the reinforcement on their mechanical behavior ought to be clearly understood. Very little information is available on the correlation between the consolidation conditions, and fiber characteristics and mechanical properties. This research has focused on the effects of

consolidation time, consolidation temperature, fiber draw ratio and fiber weight fraction on creep, fatigue and dynamic mechanical behavior of SRPPCs. Analysis of the creep, dynamic mechanical and fatigue measurements of SRPPCs is expected to provide more insight into molecular chain interactions due to the highly oriented fibers, and fiber loading.

1.3 Objectives of the study

1.3.1 Main objective

The main aim of this research was to fabricate self-reinforced PP composites using PP films and fibers of various draw ratios and investigate their mechanical behavior and thermal stability.

1.3.2 Specific objectives

The specific objectives of this work were to investigate the effects of:

i. Consolidation temperature on dynamic mechanical properties, fatigue, creep response and thermal stability of self-reinforced polypropylene composites,
ii. Consolidation time on dynamic mechanical properties, fatigue, creep response and thermal stability of self-reinforced polypropylene composites,
iii. Fiber weight fraction on dynamic mechanical properties, fatigue, creep response and thermal stability of self-reinforced polypropylene composites,
iv. Fiber draw ratio on dynamic mechanical properties, fatigue, creep response and thermal stability of self-reinforced polypropylene composites.

1.4 Rationale of the study

Mechanical properties of polypropylene have always been improved by adding glass fibers. These fibers are heavy due to the high density glass. Also coupling agents are used to increase fiber-matrix adhesion and improve interfacial strength. Recycling/reprocessing of these composites is difficult, complex and expensive, and is accompanied with loss of the good properties of the reinforcement. Self-reinforced polypropylene composite is wholly polypropylene, thus recycling of scrap /waste material from these composites is simple and cheap. In addition the need for coupling agents such as silane is completely eliminated, thus making the composite more environmental friendly. This greatly contributes towards the satisfaction of the enormous desire for green materials. Finally, favorable changes in properties without increase in density of the materials have a strong and positive impact on production of light weight components which are in high demand in various industries.

Self-reinforced polypropylene composites are a relatively new class of composites and have been found to have good properties. The properties of these composites differ when processing conditions and characteristics of the reinforcement are varied. Therefore, greater understanding of their behavior is gained by investigating the effects of these variations on the mechanical properties of self-reinforced polypropylene composites.

CHAPTER TWO

LITERATURE REVIEW

2.1 Introduction

In this chapter re-processability of polypropylene, PP based composites, and past works done on polypropylene based composites will be reviewed. At first, a discussion on the re-processability of polypropylene will be given. Thereafter, polypropylene based composites will be overviewed and compared to self-reinforced polypropylene composites. Finally, related studies on self-reinforced PP composites will be presented.

2.2 Re-processability of polypropylene

Several researchers have shown that PP can be re-processed several times without significant loss of important properties (Talreja, 1987; González-González *et al*., 1998; Incarnato *et al*., 1999; Xiang et al., 2002; Ramírez-Vargas *et al*., 2004; Rust *et al*., 2006; Da Costa *et al*., 2007). According to Martins *et al.* (2002), molar mass and viscosity of pure and post-consumer PP were found to decrease with molding (reprocessing) cycles. The decrease is due to degradation by chain scission, caused by heat loading and mechanical shearing. However, use of an antioxidant leaves the properties unchanged.

Da Costa *et al.* (2007) showed that the number of processing cycles has minor negative effects on mechanical properties. Several other studies reported no or only a slight decrease in the tensile strength and in the molecular weight of the material (Incarnato *et al*., 1999; Ramírez-Vargas *et al*., 2004; Rust *et al*., 2006). But,

improvement in the impact properties and the elongation at break occurred after reprocessing. After several reprocessing cycles there was no significant change in the chemical structure and average molecular weights of PP (González-González *et al.*, 1998; Xiang *et al*., 2002).

2.3 Polypropylene based composites

2.3.1 Glass fiber reinforced PP composites

Long discontinuous fiber reinforced materials, known as glass mat thermoplastics (GMTs) are used commonly for compression molding (Czél *et al*., 2008). Although GFs are available with different polymer matrices, in several cases with thermosets, the market is dominated by PP based GMTs due to their low price (see Appendix A to D) (Thomason *et al*., 1999; Karger *et al*., 1999; Fibre Glast Development Corporation, http://www.fibreglast.com).

The stiffness, tensile strength and impact strength of GFRPPCs increase almost linearly with fiber concentration up to 40 wt % (for stiffness) and 60 wt % (for tensile strength). Tensile and impact properties increase with fiber length (Thomason *et al*., 1996). However, the stiffness is independent of fiber length above 0.5 mm. High concentrations of long fibers (> 40 wt %) results in fiber packing problems and increase void content which leads to a reduction in modulus (stiffness). Thus packing of fibers depends on fiber length (Thomason *et al*., 1996, 1997).

Bonding between the polymer and the reinforcement determines the quality of mechanical properties of composites. To achieve good interfacial connection, coupling agents such as silane are most widely used. However, coupling GFs to PP is difficult due to the non-polar nature of PP. Thus, another additive, often PP grafted with maleic anhydride (PP-g-MA) is used (Gibson *et al*., 1995; Hamada *et al.* 2000).

2.3.2 Other fiber-reinforced PP composites

Basalt fiber (BF) is one of the materials used as reinforcement for polymeric composites. BFRPP composites have high tensile strength especially when a coupling agent is applied (Botev *et al.*, 1999; Czigány *et al*., 2008; Deák *et al*., 2009, 2010).

Natural fiber (NF) reinforced composites gained ground due to the disadvantages of GF. The mostly used NFs are hemp, sisal and flax (Mieck *et al*., 1999). They have good mechanical properties, are available worldwide, and the production of these reinforcements is cheap. Garkhail *et al.* (2000) made flax reinforced PP composites by film-stacking method. According to these researchers, tensile strength and modulus increase with fiber length. These properties are enhanced even more with the use of a coupling agent (maleic anhydride). With increased fiber content, the modulus increases and compares favorably with values of GFRPP composites.

2.4 Re-processability of polypropylene based composites

Being a commodity plastic polypropylene has to be filled and reinforced in order to compete with engineering plastics. In order to improve the properties of PP, glass fiber (GF) is commonly used (Izer *et al*., 2010). The use of inorganic reinforcements, such as glass fibers makes thermoplastics difficult to recycle. Reprocessing of GFRPP composites is accompanied with substantial loss in the properties due to breakage of the reinforcing GF (Barkoula *et al*., 2008). The use of inorganic reinforcements, such as glass fibers, makes thermoplastic composites no longer recyclable and very heavy due to the high density glass fibers. To meet the demand for recyclable fiber reinforced polymer composites, fibers which can be melted along with the polymer matrix and be compatible with that melt have been proposed by several researchers (Klein *et al*., 1995; Stern *et al*., 1997; Nuriel *et al*., 2000; Kitayama *et al*., 2000; Fukui *et al*., 2002; Vaisman *et al*., 2003; Fukui *et al*., 2004; Cabrera *et al*., 2004).

Recycling of hemp and sisal fiber reinforced PP composites reduces fiber length due to the injection and grinding process. Although use of a coupling agent improves the fiber-matrix adhesion, its effect disappears with increased cycling (Bourmaud *et al*., 2007). Similarly, reprocessing of wood fiber reinforced PP composites damages the fiber. Overall, this process of recycling natural fiber composites significantly deteriorates the mechanical properties (Beg *et al*., 2008; Srebrenkoska *et al.* 2008).

2.5 Self-reinforced composites

From the preceding sections, inorganic fibers (GF, BF), and natural fibers improve the mechanical properties of PP-based composites. However, the drawbacks of these composites are the poor interfacial strength between the reinforcement and the matrix that requires the addition of coupling agents. Another disadvantage is the difficult recycling since the valuable reinforcement cannot be recovered economically as the separation of the reinforcement and matrix has not been solved. On the other hand, thermoplastic composites lose their excellent mechanical properties after reprocessing due to the breakage of fibers. To overcome these problems, a good alternative is the application of self-reinforced polymer composites in which the matrix and the reinforcement are chemically compatible. The advantages of these composites are the good mechanical properties and the easy recyclability owing to the thermoplastic polymer components. The challenge is to find a suitable processing window that is large enough to keep the oriented fibers intact while being impregnated with the matrix (Izer *et al*., 2010).

The original concept of self-reinforced composite was presented about three decades ago for high density polyethylene (Capiati *et al*., 1975). Since then, self-reinforced polymers have been the subject of numerous publications focusing on a range of polymers and processing routes including, polypropylene (Ward *et al.*, 2004), polyethylene (Jordan *et al.*, 2002), polyethylene terephthalate (Rojanapitayakorn *et al.*, 2005), and liquid crystal polymers (Pegoretti *et al.*, 2006). Studies have also been presented for biomedical applications, where the self-reinforcement of polymers are

required for load bearing orthopaedic applications, without complicating biocompatibility or bio-resorption profiles (Wright-Charlesworth *et al*., 2005).

2.6 Self-reinforced composites production techniques

There are three ways to produce SRPCs, hot compaction, consolidation of coextruded tapes and the film-stacking method. The hot compaction method was developed at the University of Leeds by Ward *et al*., (1997, 2004). The essence of this process is the production of composites from oriented thermoplastic fibers without the incorporation of a resin, but using only suitable pressure and temperature. It exploits the special behavior of the constrained fibers, namely that the core and the surface melt differently when heated. The process of hot compaction is illustrated in figure 2.1. The concept of the technique is to heat an array of polymer fibers or tapes considered to be oriented at a temperature where a thin skin of the material on the surface of each fiber or tape melts. During cooling this melted material recrystallizes to form the continuous matrix of SRPCs. The residual fibers provide the reinforcement for the composite. However, hot compaction provides a narrow processing window.

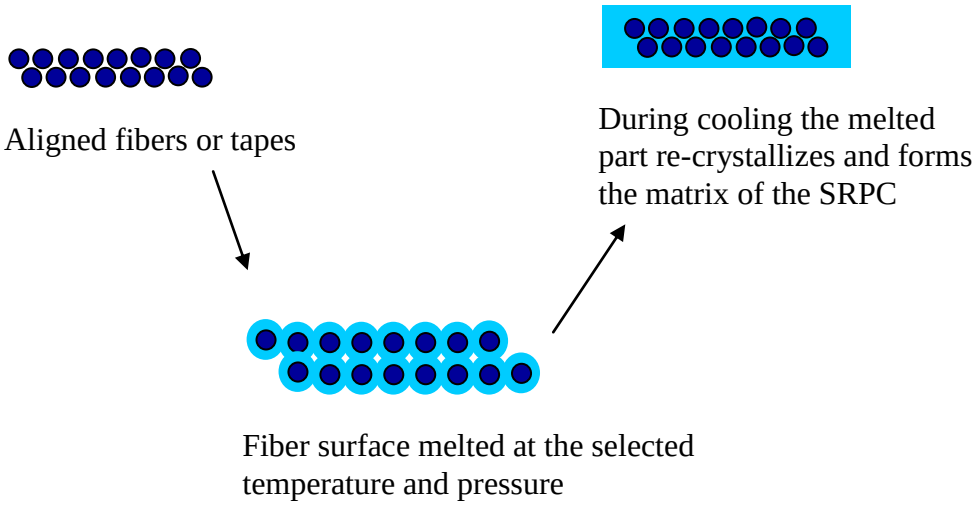

Figure 2.1: The Hot compaction method (Ward *et al*., 1997, 2004)

The consolidation of coextruded tapes method was developed by Peijs *et al.*, (2003). The process scheme is shown in figure 2.2.

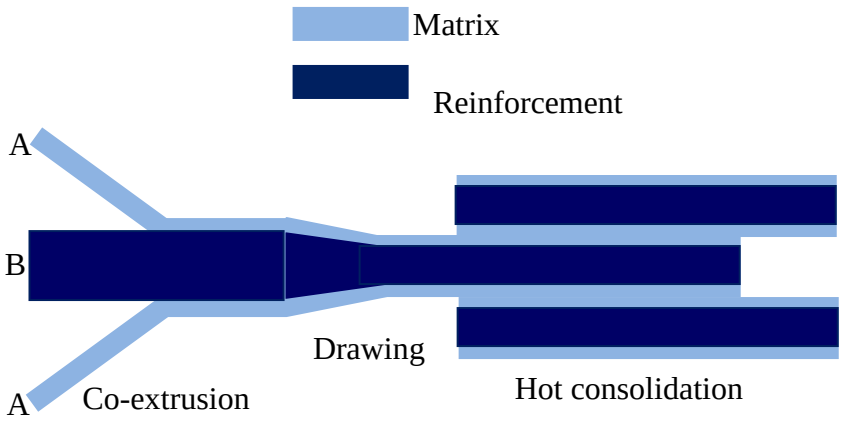

Figure 2.2: Scheme of co-extrusion process (Peijs *et al.*, 2003; Alcock *et al*., 2006)

During the co-extrusion of PP tapes, two types of PP with different melting temperatures are combined, namely a thin polymer skin with lower melting temperature than the core material (the lay-up is A/B/A). This matching of two

different PPs yields a processing window over 20°C. During hot pressing the thin surface (having lower melting temperature - A) melts and forms the matrix, while the core (B) remains oriented and acts as the reinforcement. A high fiber volume fraction (>80%) can be achieved with this technique.

Self-reinforced polymer composites with excellent mechanical properties can be manufactured with afore mentioned techniques, however they are difficult and expensive. The film-stacking method (Figure 2.3), gives a possibility to combine even commercially available pre-products (films, fibers) together. The scheme of the film-stacking method is shown in figure 2.3.

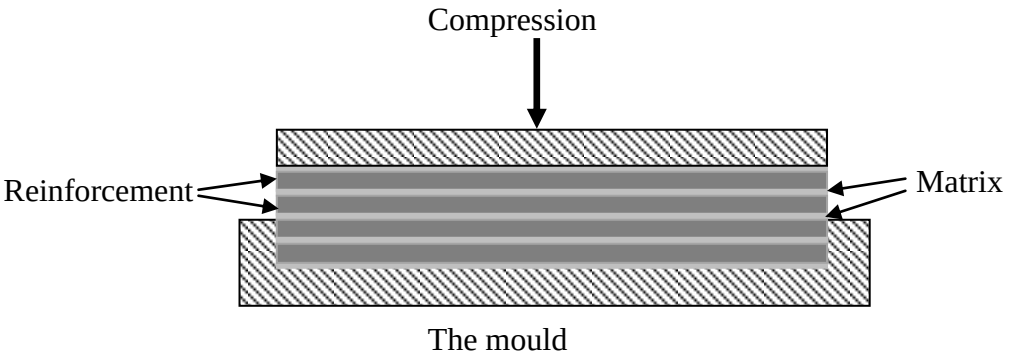

Figure 2.3: Film-stacking technique (Houshyar *et al*., 2003, 2004)

Based on the concept of this technique, the reinforcement and the matrix layers are placed on each other alternately prior to consolidating them into composites by hot pressing. The key issue is the same as for the previously presented techniques, i.e. the melting temperature difference between components, as the reinforcement should keep its strength while the matrix melts and cools (Houshyar *et al*., 2003, 2004).

2.7 Related studies

Optimum compaction of SRPPCs is achieved when sufficient amount of polymer melts to fill all the cavities and make the resulting SRC a continuous material (Hine *et al*., 2008; Teckoe *et al*., 1999). At lower compaction temperatures not all voids are filled, whereas, higher compaction temperature melts more material than is required. As the compaction temperature increases, the percentage of melted material also grows. Thus, bonding improves and hence the modulus and strength increase (Hine *et al*., (2003). With increasing molding pressure, the matrix melts and penetrates the reinforcement better. Consequently, processing time as well as fiber shrinkage is reduced (Houshyar *et al.,* 2006).

According to Houshyar *et al*. (2004) and Alcock *et al.* (2007) processing pressure and temperature influence the structure and the mechanical properties of SRPPCs. Higher pressure results in proportionally better mechanical properties, while the interfacial strength increases with increasing processing temperature. Specimens consolidated at 140°C fail by fiber/matrix debonding and inter-laminar shearing. However, the specimens manufactured by hot pressing at 160°C fail due to fiber breakage. With increasing consolidation temperature, the peel strength also increases courtesy of interfacial tests. On the other hand, impact performance of SRPPCs increase with decreasing processing temperature and pressure (Alcock *et al*., 2006; 2008).

The mechanical behavior of self-reinforced polymer composites depends on the reinforcement architecture of the composites. All-PP composites reinforced uni-

directionally offer greater resistance to creep compared to the cross-ply ones. The unidirectional (UD) architecture significantly improves the elastic recovery of the composite. The stiffness of the SRPPCs is to a great extent governed by the stiffness of the fibers (or tapes) in the longitudinal direction. On the other hand, the CP composites exhibit higher void content and slightly lower crystallinity (Alock *et al*., 2006; Banik *et al*., 2007; 2008). PP fibers woven into satin fabric geometry have a positive influence on mechanical properties. This geometry offers the advantage of loose pattern and high fiber content (Houshyar *et al*., 2005). Use of interleaved films increases the interfacial strength, improves thermoformability and offers the benefit of a wider processing window (Hine *et al*., 2008).

Composites produced by the film stacking technique with PP fibers and random PP copolymer (rPP) matrix have their modulus increased with increasing fiber diameter (Houshyar *et al*., 2003). With an increasing fiber diameter the total interfacial area of the composites decreases. Consequently, the adhesion between the matrix and the reinforcement is excellent due to perfect wetting. In terms of fiber loading, Houshyar *et al.* (2005) have shown that tensile, flexural, and storage moduli increase considerably with increasing fiber concentration. The maximum improvement in properties is observed for the composite with a fiber content of 50 wt%, defined as the critical fiber concentration. This was due to increasing void content and fiber packaging problems in case of 60 wt% fiber content.

In their work, Bárány *et al.* (2006) used PP carded mat as reinforcement and β-crystal form of PP homopolymer (β-PP) film as matrix. The composite plates were

manufactured at different processing temperatures (150-170°C) and high pressure (7 MPa) with a nominal reinforcing content of 50 wt%. It was concluded that with increasing processing temperature the laminate-like lay-up progressively disintegrated. Good consolidation was achieved at high processing temperature. The tensile and peel properties increased, delamination during failure was hindered while the impact characteristics decreased.

Abraham *et al.* (2008) manufactured all-PP composites by exploring the polymorphic forms of PP, in which α-rPP homopolymer tapes worked as reinforcement and β-nucleated random PP copolymer (c) as matrix. Both unidirectional (UD) and cross-ply (CP) laminates were prepared by tape winding technology combined with a film stacking method followed by hot pressing. The mechanical performance of the composites was investigated by dynamic mechanical thermal analysis (DMTA), static flexural and dynamic impact tests. Both the DMTA and the static flexural bending tests revealed that the α-PP tape acted as a more effective reinforcement for the β-rPP matrix than for the α-rPP especially for all-PP composites of UD lay-up. The perforation impact properties were determined from instrumented falling weight impact (IFWI) tests, performed at room temperature. It was found that transcrystalline layer is responsible for the stress transfer from the β-rPP matrix to the α-PP reinforcement

The creep behavior of all-PP composites processed by film stacking method was investigated in different compositions using different molding conditions (Houshyar *et al*., 2006), different ethylene-propylene elastomer (EP) concentrations (Houshyar

et al., 2007) and different fiber diameters (Houshyar *et al*., 2004, 2005). It was concluded that the creep behavior of PP fiber reinforced PP composites depended strongly on stress, temperature, void content, and fiber loading. The composite produced under optimum molding conditions (where the wetting of fibers was complete) showed the lowest relative creep. Creep resistance decreased if temperature or stress rose.

Creep testing is a basic probe of polymer relaxations and a fundamental form of polymer behavior. Creep phenomenon is of importance for material applications requiring long-term durability and reliability (Aifantis, 1987; Sosa, 1994; Krempl *et al*., 2003). As an inherent defect, creep deformation causes poor dimensional stability of thermoplastics, thus it is a serious problem (Morra *et al*., 2009). In this research, the creep behavior of self-reinforced PP composites as a function of consolidation temperature, consolidation time, fiber draw ratio and fiber weight fraction was investigated.

During the past several years, thermoplastic polymers and their composites have found increasing number of applications in structures that are subjected to cyclic or fatigue loading (Agarwal *et al*., 2006; Ţăranu, 2009; Herakovich, 1998; Bunsell *et al*., 2005). Many of these structures may experience low amplitude vibrations over extended periods of time, and are therefore prone to unexpected fatigue failure in service. Since fatigue failure is a major concern in designing these structures, it is important to establish the fatigue properties of polymers to be used in these structures. The potential application areas of SRPPCs being enormous including

automotive industry among others, understanding the fatigue behavior of these composites is of great significance.

Several approaches can be employed during fatigue studies such as those based on the number of de-bonded fibers, fracture mechanics parameters, the strain energy density, and the loss of stiffness (Joseph *et al*., 1994; Echtermeyer *et al*., 1995; Ferreira *et al*., 1996, 1997) and fatigue strength (Spearing *et al*., 1994). In this research loss of stiffness was used to analyse fatigue behavior (damage) of self-reinforced PP composites under cyclic loading.

Despite the extensive work that has been done in this area of self-reinforced polymer composites, there does not seem to be any systematic study reporting on the optimization of the composites consolidation conditions and fiber characteristics, and their effects on dynamic mechanical properties, creep behavior fatigue and thermal decomposition. This formed the subject of this study and the polymer to be studied was polypropylene.

CHAPTER THREE

THEORETICAL ASPECTS OF THE MEASUREMENT TECHNIQUES

3.1 Introduction

This Chapter gives details of the theories behind the various tests carried out in this research. First dynamic mechanical analysis as a measurement technique is explained. Thereafter, the theory of the dynamic mechanical analyser as a test equipment is given. Detailed descriptions of the various models relevant to the study and analysis of experimental results follow, ending with the theory of thermal decomposition of polymers.

3.2 Dynamic Mechanical Analysis

3.2.1 Dynamic Mechanical Analysis (Measurement technique)

Dynamic mechanical analysis (DMA)-is a thermal analysis technique that measures the properties of materials as they are deformed under periodic stress. A variable sinusoidal stress is applied, and the resultant sinusoidal strain is measured. If the material being evaluated is purely elastic, the phase difference between the stress and strain sine waves is 0° (i.e., they are in phase). If the material is purely viscous, the phase difference is 90°. However, most real-world materials including polymers are viscoelastic and exhibit a phase difference between those extremes. This phase difference, together with the amplitudes of the stress and strain waves, is used to determine a variety of fundamental material parameters, including storage and loss modulus, damping (tan δ), transition temperatures, and creep (Menard, 1999; Hevin *et al*., 2008).

3.2.2 Dynamic mechanical analyser (Instrumental considerations)

The dynamic mechanical analyser is the instrument that performs the dynamic mechanical analysis test. The DMA 2980 dynamic mechanical analyser is designed to optimize the combination of these critical components. The DMA 2980 offers a broad range of deformation modes, as well as a variety of clamp sizes so that sample materials ranging from single fibers to films and bars, including viscous liquids can be accommodated (Ferry, 1980; McCrum *et a*l., 1991; Ward *et al*., 1993; Reading, 1995; Price, 2002).

3.2.3 Dynamic Mechanical Analysis (the complex modulus)

Dynamic mechanical properties refer to the response of a material as it is subjected to a periodic force. These properties may be expressed in terms of a dynamic modulus, a dynamic loss modulus, and a mechanical damping term. For an applied stress varying sinusoidally with time, a viscoelastic material will also respond with a sinusoidal strain for low amplitudes of stress.

The strain of a viscoelastic body is out of phase with the stress applied, by the phase angle, δ. This phase lag is due to the excess time necessary for molecular motions and relaxations to occur (Ferry, 1980; Ward *et al*., 1993). Dynamic stress, σ, and strain, ε, are given as:

$$\sigma = \sigma_o \sin(\omega t + \delta) \quad (3.1)$$

$$\varepsilon = \varepsilon_o \sin(\varpi t) \quad (3.2)$$

where ω is the angular frequency. Using this notation, stress can rewritten as,

$$\sigma = \sigma_o \sin(\omega t) \cos\delta + \sigma_o \cos(\omega t) \sin\delta. \quad (3.3)$$

Dividing stress by strain to yield a modulus and using the symbols E´ and E´´ for the in-phase (real) and out-of-phase (imaginary) moduli yields:

$$E^* = E^{'} + E^{''} \tag{3.4}$$

where E′ is the storage modulus (stiffness) and E'' is the loss modulus (internal friction). The phase angle δ is given by;

$$\tan\delta = \frac{E^{''}}{E^{'}} \tag{3.5}$$

(Ward *et al*., 1993; Ferry, 1980).

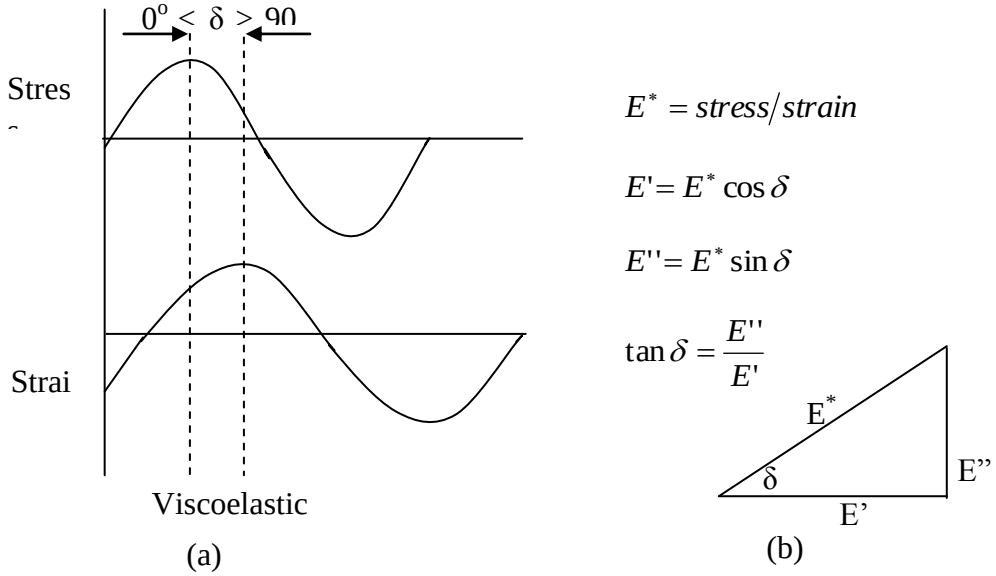

Figure 3.1: (a) Phase lag δ, between stress and strain for viscoelastic material (b) Relationship between complex modulus E*, storage modulus E', loss modulus and phase angle, δ (Ferry, 1980; Ward *et al*., 1993).

3.3 Fatigue

Fatigue is the failure or decay of mechanical properties after repeated application of stress or strain. It has been estimated that fatigue contributes to approximately 90% of all mechanical service failures. Most notably, failure can occur if the applied stress

exceeds the strength limits of the material. Failure may also be attributed to material property deficiencies resulting from improper processing conditions that lead to defects (such as gas or shrinkage pores, inclusions, and weld-and-flow-line defects) (Mitchel, 1996; Kaplan *et al*., 2002; Flake, 2008).

3.3.1 Stress Cycles

There are three basic factors necessary to cause fatigue. They include:

- a maximum tensile stress of sufficiently high value,
- a large enough variation or fluctuation in the applied stress, and
- a sufficiently large number of cycles of the applied stress.

A fully reversed stress cycle, such as the one shown in figure 3.2, where the maximum and minimum stresses are equal, is commonly used in testing of fatigue (Kaplan *et al*., 2002; Flake, 2008).

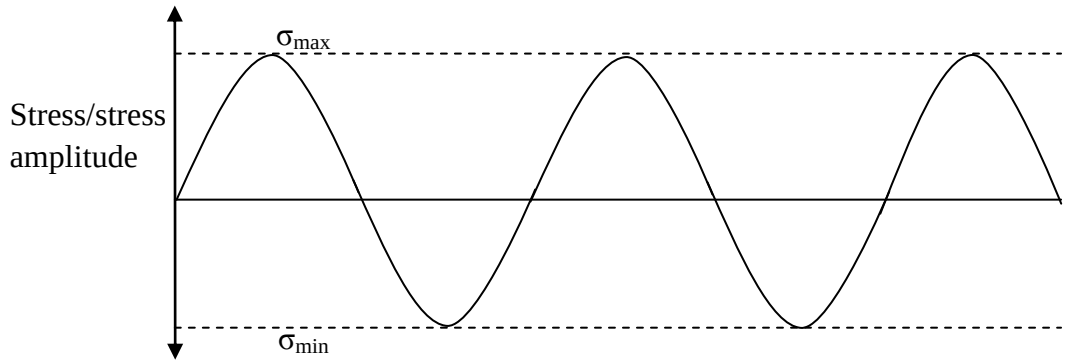

Figure 3.2: Typical fully reversed loading cycle (Flake, 2008)

Two ratios frequently used in presenting fatigue data are stress ratio, R, (equation 3.6), and amplitude ratio, A, (equation 3.7) (Kaplan *et al*., 2002; Flake, 2008).

$$R = \frac{\sigma_{\max}}{\sigma_{\min}} \tag{3.6}$$

$$A = \frac{1+R}{1-R} \tag{3.7}$$

3.3.2 Fatigue damage

Failure of a component due to fatigue generally occurs through a two-step process. The first step involves the initiation of microcracks or other damage at inhomogeneities or defects in the material. This damage can initiate and evolve at nominal stress levels far below the yield or tensile strength of the material. This step is commonly referred to as the initiation stage. The second step involves the growth of damage through the coalescence of microcracks and the subcritical propagation of these small cracks to form large cracks and ultimately cause component failure. This step in the failure process is referred to as the propagation stage. For most polymeric materials, the initiation time can be orders of magnitude greater than the propagation time (Kaplan *et al*., 2002; Courtney, 2005; Callister, 2008; Flake, 2008).

The basic failure mechanisms of polymer composites subjected to tension-tension fatigue are matrix cracking, interface debonding, delamination, splitting, and fiber breakage (Talreja, 1987; Ye, 1989; Plumtree *et al*., 1991; Ashbee, 1993; Reifsnider, 1994; Jang, 1994). The cumulative damage as a function of the number of loading cycles may be generally described by the curve in figure 3.3.

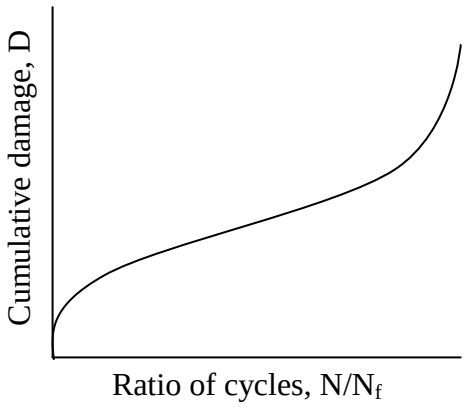

Figure 3.3: Cumulative damage as a function of number of cycles (Hai *et al*., 2000)

Matrix cracks, the first to occur in the fatigue process, are due to a high concentration of stress. As the number of cracks increases, stress redistribution reduces the initiation of new cracks, and the damage appears to grow at a constant rate as cyclic loading continues. In the region of damage, interfacial de-bonding, delamination and fiber breaking start to occur and gradually increase. Fiber breakage increases due to the continuing growth of the matrix cracks and fiber-matrix de-bonding. As the breakage progresses and intensifies, the rate of fiber fracture increases rapidly and, finally, the composite raptures.

The change in modulus has been commonly used to express the state of damage in the polymer composites (Ye, 1989; Plumtree *et al*., 1991; Subramanian *et al*., 1995; Hai *et al*., 2000) where cumulative damage, *D*, is defined (equation 3.8).

$$D = 1 - \frac{E}{E_o} \tag{3.8}$$

where E and E_o are residual and initial moduli, respectively.

The damage growth rate of composites under fatigue loading is a product of a function of the damage D and a function of mechanical environments;

$$\frac{dD}{dN} = f(D, p(N)) = f_1(D) f_2(p(N)) \tag{3.9}$$

where *p(N)* is a parameter describing the mechanical environments.

The derivative of the function rapidly decreases at the beginning, maintains at a constant as the fatigue loading continues, and then rapidly increases near the end of the life cycles, as depicted in figure 3.4.

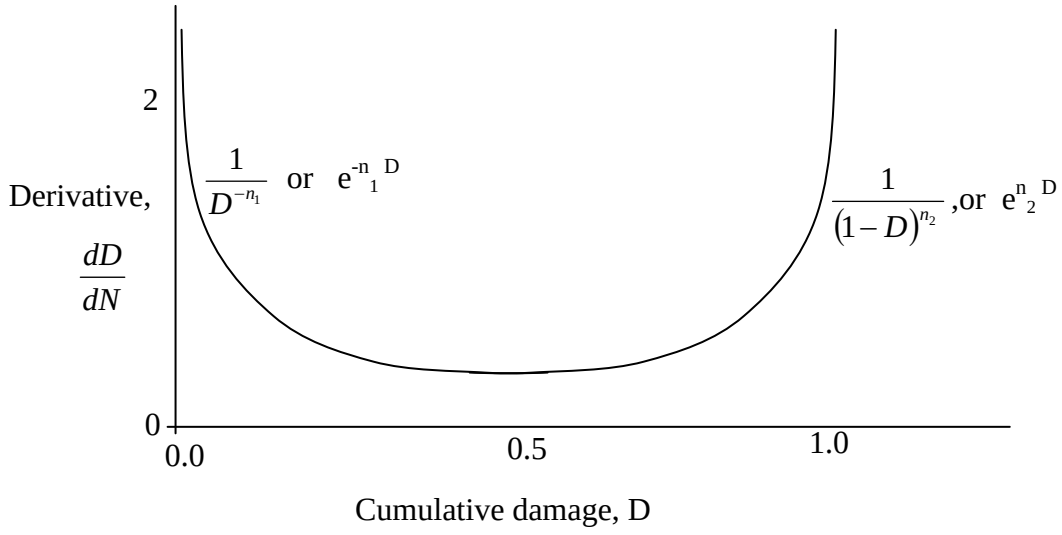

Figure 3.4: Damage growth per cycle (Hai *et al*., 2000)

The initial damage growth per loading cycle may be mathematically expressed as (Hai *et al*., 2000);

$$\frac{dD}{dN} = \frac{\chi_1}{D^{n_i}}, \tag{3.10 a}$$

or,

$$\frac{dD}{dN} = \chi_1 e^{n_i D} \tag{3.10 b}$$

Where N is the number of loading cycles; χ_1 and n_1 are the material constants at the beginning of fatigue life cycles, and $n_2 > 1$. The damage growth near the end of the life cycle before failure may be described as;

$$\frac{dD}{dN} = \frac{\chi_2}{(1-D)^{n_2}} \tag{3.11 a}$$

or

$$\frac{dD}{dN} = \chi_2 e^{n_2 D} \tag{3.11 b}$$

where, χ_2 and n_2 are material constants near the end of the fatigue life cycle before failure and $n_2 > 1$.

The general model as depicted in figure 3.4 may take the form;

$$\frac{dD}{dN} = \frac{\chi_1}{D^{n_1}} + \frac{\chi_2}{(1-D)^{n_2}} \tag{3.12 a}$$

or

$$\frac{dD}{dN} = \chi_1 e^{n_1 D} + \chi_2 e^{n_2 D} \tag{3.12 b}$$

3.4 Creep

Creep can be defined as a slow, time dependent continuous deformation (strain) of a material subjected to a constant load (stress) (Wu, 2000; Reed 2003). The deformation will progress slowly with time indefinitely or until rupture or yield causes failure. All plastics creep to a certain extent. The degree of creep depends on several factors, such as type of plastic, magnitude of load, temperature and time

(Pomeroy, 1978; Crawford, 1998). In polymers, creep occurs due to a combination of elastic deformation and viscous flow of polymer molecules, commonly known as viscoelastic deformation (Park *et al.,* 1998). Thus, when a polymer is stressed, it responds by exhibiting viscous flow (which dissipates energy) and by elastic displacement (which stores energy). This time dependent behaviour (viscoelasticity) of materials is also an important characteristic of reinforced plastics.

3.4.1 Creep stages

Figure 3.5 shows schematic curves of the various stages of creep at (a) a constant applied stress, (b) by creep strain, for polymers. According to the curve the entire processes of creep in polymers can be considered as four stages, namely (I) instantaneous deformation, (II) primary creep, (III) secondary creep, and (IV) tertiary creep (ASTM D 2990-01, 2001). The instantaneous strain is due to the elastic or plastic deformation of polymer once the external load is applied, this stage is independent of time. In the primary creep stage, the creep rate starts at a relatively high value, and decreases rapidly with time, which may be resulting from the slippage and orientation of polymer chains under persistent stress. After a certain period of time, the creep rate reaches a steady-state value in the secondary creep stage, in which the viscoelastic flow in the polymer occurs and the duration is relatively very long if under low stress level. Finally, the material falls into the tertiary creep stage, where the creep rate increases rapidly and final creep rupture or advanced necking occurs (Reed, 2003).

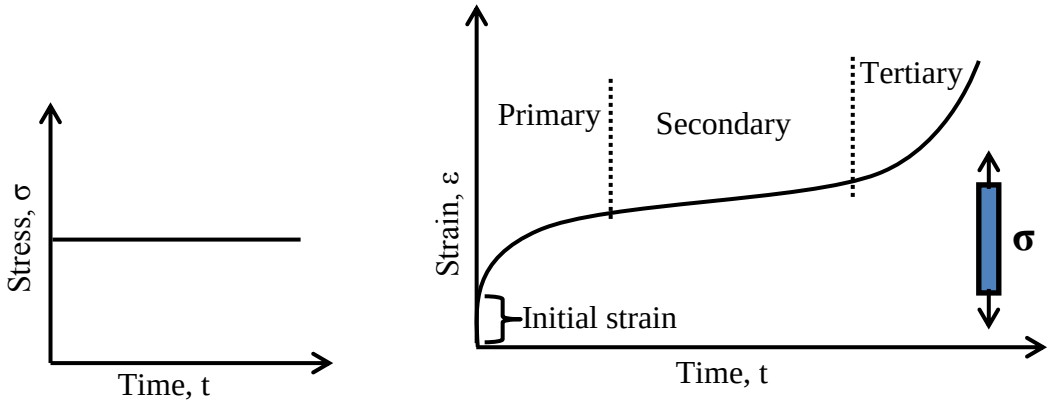

Figure 3.5: (a) Constant load applied (b) creep stages by strain (Wu, 2000; ASTM D 2990-01, 2001; Reed, 2003)

Creep compliance, J(t,s(t),T), is also frequently applied to describe the creep performance. In general, for a constant stress, σ, the creep compliance *J*(t) can be written as the ratio of the strain (ε) to the stress at a constant time (t) as follows (Pegorreti *et al*., 2006):

$$J(T,t) = \frac{\varepsilon(T,t)}{\sigma}. \tag{3.13}$$

3.4.2 Creep models

Besides experimental observations, creep modelling can be applied to polymeric materials to develop comprehensive understanding of the creep deformation phenomena. In the past half century, numerous creep models have been proposed and applied to describe the creep behaviour of viscoelastic materials (Findley *et al*., 1989; Ward, 1993; Pegorreti *et al*., 2006). The creep-recovery curve can be looked at as a combination of springs (elastic sections) and dashpots (viscous sections). The qualitative form of the basic constitutive equation for creep models is:

$$\varepsilon = \varepsilon_o + \varepsilon_c \tag{3.14}$$

where ε is the total strain at some time, t, after a stress application, ε_c, time-dependent creep component of strain at t, and ε_o is the instantaneous strain after stress application. The instantaneous strain component (ε_o) is elastic and the creep component, ε_c, is a simple arithmetic function of time (linear, logarithm, exponential, power law), either alone or in combination.

3.4.2.1 Burgers model

The Burger's model is one of the most widely used models. It gives the relationship between the morphology of the composites and their creep behaviour (Ward, 1983; Findley *et al*., 1989; Tschoegl, 1989). Burgers model consists of Maxwell and Voigt-Kelvin units combined in series. Figure 3.7 shows a scheme of the four-element Burger model and the curve which results from it. The curve shows the same regions as seen in real materials, including a small instantaneous region, a levelling off of the equilibrium region, and a realistic recovery curve. This model addresses the limitations of the two models described before.

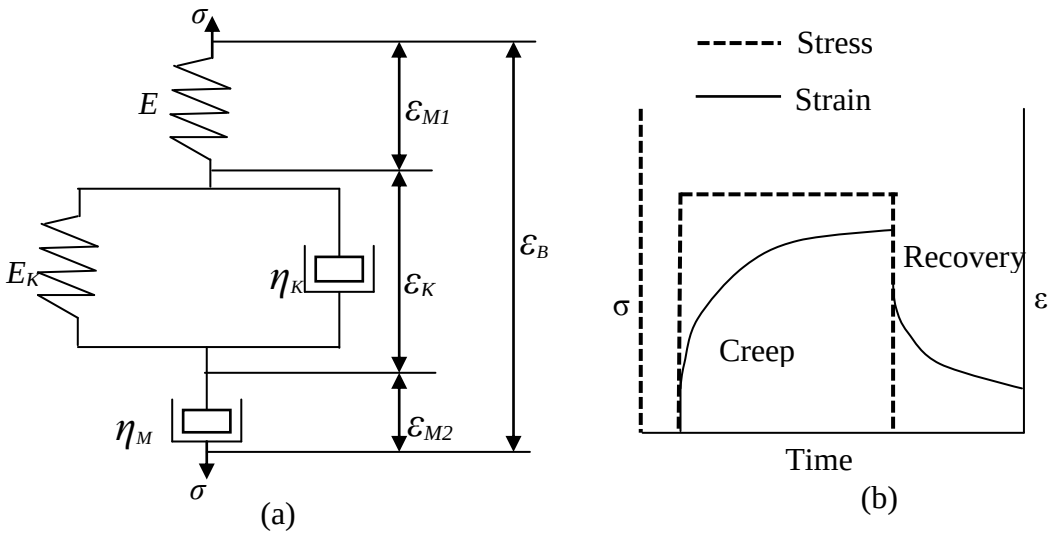

Figure 3.6: Schematic diagram of (a) Burger's model, (b) Burger's model strain curve (Tschoegl, 1989; Peng *et al*., 2011)

The constitutive equation for a Burger's model can be derived by considering the strain response under constant stress of each coupled element in series as depicted in figure 3.8. The total strain ε_B at time t is the sum of the strains in these three units, where the spring and dashpot in the Maxwell model are considered as two elements (Marcovich *et al.*, 2003; Acha *et al*., 2007), thus:

$$\varepsilon_B = \varepsilon_{M1} + \varepsilon_{M2} + \varepsilon_K \tag{3.15}$$

Which yields;

$$\varepsilon_B = \frac{\sigma_o}{E_M} + \frac{\sigma_o}{E_K}\left(1 - e^{\frac{-t\eta_K}{E_K}}\right) + \frac{\sigma_o t}{\eta_M} \tag{3.16}$$

The first term in equation (3.16) is constant and describes the instantaneous elastic deformation; the second one is delayed elasticity of the Kelvin unit and is dominant in the earliest stage of creep, but soon goes to a saturation value close to $\frac{\sigma_o}{E_K}$ (when t $\to \infty$, $\left(e^{\frac{-t\eta_K}{E_K}}\right) \to 0$); the viscous flow then increases nearly linearly in the third term after a sufficient long time period of loading. The Burgers model, which includes the essential elements, can be applied satisfactorily to model the practical behaviours of viscoelastic materials. The material parameters E_M , η_M , E_K and η_K can be simulated from the experimental data (Ward, 1983; Findley *et al*., 1989; Banik *et al*., 2008).

Differentiating equation (3.16) yields the creep rate $\left(\dot{\varepsilon}_B\right)$ of the Burgers model,

$$\dot{\varepsilon}_B = \frac{\sigma_o}{\eta_M} + \frac{\sigma_o}{\eta_K} e^{-t\frac{\eta_K}{E_K}} \tag{3.17}$$

At sufficient long time scale, the creep rate reaches asymptotically to a constant value;

$$\dot{\varepsilon}_B = \frac{\sigma_o}{\eta_M} \tag{3.18}$$

(Ward, 1983; Findley *et al*., 1989; Banik *et al*., 2008).

3.4.2.2 Findley power law model

Besides the constitutive models, empirical mathematical descriptions have also been widely studied due to their simple expression and satisfactory simulation and prediction capability. Among these, the Findley power law model is commonly accepted. The constitutive equation (3.19) proposed by Findley (Findley *et al.*, 1989), can describe the creep behaviour of many polymers with good accuracy.

$$\varepsilon_F = \varepsilon_o + \varepsilon_c t^n \tag{3.19}$$

where the subscript F indicates the parameter associated with the Findley power law; n is a constant independent of stress and generally less than one; ε_o is the time-independent strain; ε_c is the coefficient of time-dependent term; ε_o is a function of stress and environmental variables including temperature and moisture content; t is creep time. Rearranging equation (3.19) and taking logarithms leads to:

$$\text{Log}\,(\varepsilon_F - \varepsilon_o) = \log \varepsilon_c + n \log t \qquad (3.20)$$

Thus, when log (ε_F - ε_o) is plotted versus log t, a straight line with slope n and using the intercept on log (ε_F - ε_o) axis, ε_c can be determined. The power law has been widely applied to express stress-strain-time relationship for viscoelastic materials (Findley, 1989).

Differentiating equation (3.19), yields the creep rate of the Findlay power law;

$$\dot{\varepsilon}_F = \frac{n\varepsilon_C}{t^{1-n}} \qquad (3.21)$$

Here, when the creep time, $t \to \infty$, $\dot{\varepsilon}_F(\infty) \to 0$. This case is available for the polymers that do not exhibit a pronounced secondary stage, especially for the case under low stress level (Findley *et al.*, 1989).

3.5 Time-temperature superposition principle (TTSP)

One of the greatest constrains in studying the viscoelastic behaviour of polymers is the relatively long time required for performing a test. Hence, methods that are able to predict long-term data have gained considerable attention. Several observations show that the effects of time and temperature are equivalent. The related time-temperature superposition principle is one of the most widely used extrapolation technique that has been applied to virtually every mechanical property and each kind of plastic. TTSP implies that the viscoelastic behaviour at one temperature (T_{ref}) can

be related to that at another temperature by a shift, a_T, in time-scale only (equation 3.22) (William *et al*., 1955; Ward, 1983; Banik *et al*., 2007).

$$\dot{t} = \frac{t}{a_T} \tag{3.22}$$

where $\dot{t}$ is the shifted, or reduced, time; t is the elapsed time of a test and a_T is the shift factor specific to a test.

For any reference temperature chosen, a fully overlapped continuous curve called a master curve is formed. This master curve can be used to predict the viscoelastic performance over long time scale. The master curve can also be used to determine the time at which a particular viscoelastic quantity reaches some critical value. TTSP can be used to obtain the master curves for several properties such as creep, creep compliance, and stress compliance versus time (or log (t)) or dynamic modulus against frequency (Fung, 1972; Lai *et al*., 1995; Rowe *et al*, 2003; Alwis *et al*., 2006).

The shift factor is usually described either by the Williams-Landel-Ferry (WLF) equation or the Arrhenius relationship. The WLF equation, is described as

$$\log a_T = -\frac{C_1(T - T_o)}{C_2 + (T - T_o)} \tag{3.23}$$

where C_1 and C_2 are constants dependent on the nature of the material, T is the test temperature and T_o is the reference temperature (C_1=17.4 and C_2=51.6°K if, $T_o = T_g$).

The use of WLF equation is restricted to materials above the glass transition temperature (Alwis *et al.*, 2006) or in the glass transition region (Thermal Analysis & Rheology, 2007). The equation is based on the assumption that, above the glass transition temperature, the fractional free volume increases linearly with respect to temperature. The model also assumes that as the free volume of the material increases, its viscosity rapidly decreases (Thermal Analysis & Rheology, 2007).

However, some materials do not display a glass transition, but remain crystalline at all temperatures. The relationship between the temperature and the horizontal shift factor, log (a_T), for materials that do not display glass transition or for those that are being studied below the glass transition temperature is based on the Arrhenius equation:

$$\log a_T = \frac{\Delta E_a}{2.303R}\left(\frac{1}{T} - \frac{1}{T_o}\right) \tag{3.24}$$

where R is the universal gas constant and ΔE_a is the activation energy, and can be obtained from the slope of the curve of log a_T against 1/T. It is fairly believed that TTSP manifests itself from the molecular behaviour and, therefore, equations based on the activation energy, such as the Arrhenius equations are proposed (Banik *et al.*, 2007).

3.6 Thermal decomposition of polymers

Solid polymeric materials undergo both physical and chemical changes when heated. This usually results in undesirable changes to the properties of the material. Thermal

decomposition is “a process of extensive chemical species change caused by heat.” (ASTM E 176, 1995). During thermal decomposition, polymers undergo chemical and physical processes. The chemical processes are responsible for the generation of flammable volatiles while physical changes, such as melting and charring, can markedly alter the decomposition and burning characteristics of the material. The chemical composition of polymers indicates their reactivity and their mechanism of thermal decomposition (Philip *et al*., 2002).

The various physical processes that occur during thermal decomposition can depend on the nature of the material. For example, as thermosetting polymeric materials are infusible and insoluble, once formed, simple phase changes upon heating are not possible. Thermoplastics, on the other hand, can be softened by heating without irreversible changes to the material, provided heating does not exceed the minimum thermal decomposition temperature. This provides a major advantage for thermoplastic materials in the ease of moulding and thermoforming of components (Philip *et al*., 2002; Craig *et al*., 2008).

The physical behaviour of thermoplastics in heating is dependent on the degree of order in molecular packing, (i.e., the degree of crystallinity). For crystalline materials, there exists a well-defined melting temperature. When designing a material, there are several techniques that can be utilized to increase the temperature at which physical transformations occur. These strategies are generally aimed at increasing the stiffness of the polymer or increasing the interaction between the polymer chains. It is clear that increasing the crystallinity of the polymer increases

the interaction between polymer chains. In the highly ordered state associated with crystalline materials, it is less possible for polymer chains to move relative to one another, as the additional forces must be overcome in the transformation to the unordered fluid state. Crystallinity is enhanced by symmetric regular polymer structure. Regular structure allows adjacent polymer chains to pack in a regular and tight fashion. Melting temperatures can also be increased by increasing the interaction between polymer chains or by chain-stiffening. Chain stiffening may be accompanied by suitable thermal stability and oxidation resistance in order to achieve increased service temperatures (Philip *et al*., 2002; Craig *et al*., 2008).

The thermal decomposition of polymers may proceed by oxidative process or simply by the action of heat. In many polymers, the thermal decomposition processes are accelerated by oxidants (such as air or oxygen). In that case, the minimum decomposition temperatures are lower in the presence of an oxidant. Among simple thermoplastics the most common reaction mechanism involves the breaking of bonds in the main polymer chain (Philip *et al*., 2002; Craig *et al*., 2008).

For polypropylene, upon thermal decomposition, very little monomer formation is observed; it forms a large number of different small molecules (up to 70), mostly hydrocarbons. Thermal stability of polyolefins is strongly affected by branching, with linear polyethylene most stable and polymers with branching less stable (Figure 3.7).

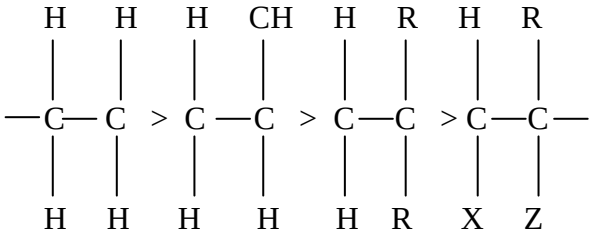

Figure 3.7: Order of thermal stability for polyolefins with respect to branching

where, R is any hydrocarbon group larger than a methyl group (Craig *et al*., 2008).

In polypropylene, every other carbon atom in the main chain is a tertiary carbon, which is thus prone to attack. This lowers the stability of polypropylene as compared to polyethylene. Chain scission and chain transfer reactions are important during thermal decomposition. Reductions in molecular weight are first observed at 500 to 520 K and volatilization becomes significant above 575 K. Piloted ignition of PP due to radiative heating has been observed at a surface temperature of 610 K. Oxygen drastically affects both the mechanism and rate of decomposition where decomposition temperature is reduced by about 200 K (Philip *et al*., 2002; Craig *et al*., 2008).

3.6.1 Thermal decomposition kinetics

In thermogravimetric analysis, the conversion rate of reaction may be defined as the ratio of actual mass loss corresponding to the degradation process (equation 3.25);

$$\alpha = \frac{M_o - M}{M_o - M_f} \tag{3.25}$$

where M, M_o, and M_f are the actual, initial and final masses of the sample, respectively (Magdalena *et al*., 2008: Fei *et al*., 2008).

The rate of decomposition, (dα/dt), can be expressed as a function of temperature and mass of the sample, i.e.

$$\frac{d\alpha}{dt} = A\exp\left(-\frac{E_{app}}{RT_a}\right)(1-\alpha)^{\beta} \tag{3.26}$$

A is the frequency factor, β is the reaction order, E_{app} is the apparent activation energy decomposition, R is the universal gas constant and T_a is the absolute temperature.

Upon introducing the heating rate, $r = (dT/dt)$, equation (3.26) becomes,

$$\frac{d\alpha}{(1-\alpha)^{\beta}} = \frac{A}{r}\exp\left(-\frac{E_{app}}{RT_a}\right)dT \tag{3.27}$$

Equation (3.27) gives the fundamental relationship to determine kinetic parameters on the basis of thermogravimetric data. The integral form of equation (3.27) is;

$$g(\alpha) = \frac{A}{r}\int_0^T \exp\left(-\frac{E_{app}}{RT_a}\right)dT = \frac{AE_{app}}{rR}\,p(x) \tag{3.28}$$

where $x = \frac{E}{RT}$ and $p(x) = -\int_{\infty}^{\frac{E}{Rx}} \frac{\exp(-x)}{x^2}\,dx$ (3.29)

(Magdalena *et al*., 2008: Fei *et al*., 2008).

CHAPTER FOUR

MATERIALS AND METHODS

4.1 Introduction

This chapter describes the materials, apparatus used and the experimental procedures applied in this study. It gives the details of the equipment that were fabricated. The various stages involved during sample preparation are also outlined. In addition, the measurement of dynamic mechanical response, creep behaviour and fatigue response are explained.

4.2 Materials

4.2.1 Polypropylene (PP)

Commercial isotactic homopolymer PP that was used as the main material was provided by General Plastics Company, located at industrial area Nairobi, Kenya. The material was in the form of round milky pellets of average diameter 3 mm. Its characteristics are as follows:

weight average molecular weight, ($\overline{M_w}$) = 50000 - 350000g/mol, number average molecular weight, ($\overline{M_n}$) = 38000-60000g/mol, polydispersity index PDI= 2.20 – 8.00, glass transition temperature, (T_g) = (-20 – (-10)) ^oC, melting point (*Tm*) = 438 - 443K and density of 0.90 – 0.91 g cm^{-3}. Its chemical structure consists of a linear repeating unit (- C_3H_6 -) $_n$, where n is the number of monomer units forming the polypropylene chain (Forstner *et al*., 2009; Wagner, 2010).

4.3 Equipment

The sample preparation apparatus consisted of the moulds, a fiber drawing machine and an oven.

4.3.1 The moulds

Two types of moulding chambers were used; the film compression moulding equipment (Figure 4.1) and the composite fabrication mould (Figure 4.2). The film making mould consisted of two thick aluminium plates measuring 8cm by 8cm and two metal bars each measuring 1cm by 0.023cm by 8cm which acted as spacers to give a uniform thickness to the film formed.

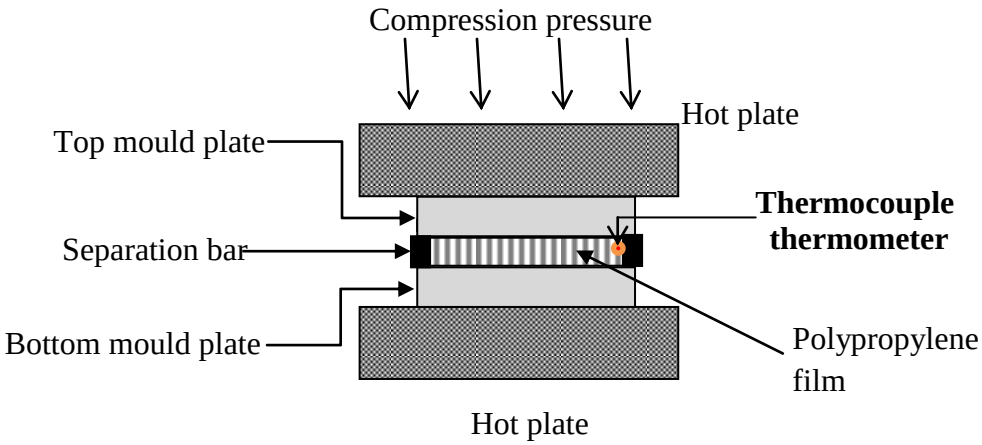

Figure 4.1: Film compression moulding apparatus

The composite fabrication mould was made of aluminium sheet shaped to form a rectangular chamber measuring 50mm by 20mm by 2.5 mm. One end of the chamber was hinged to facilitate easy opening to load the composite assembly for consolidation. The inner spacing was enough to accommodate the composite material and the thermometer to monitor the moulding temperature.

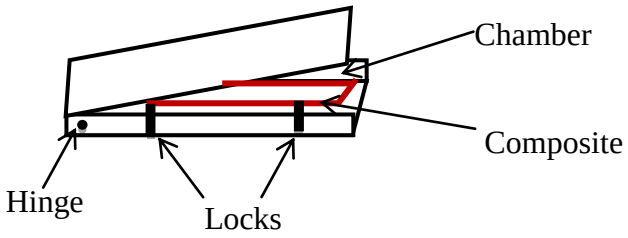

Figure 4.2: Composite fabrication mould

4.3.2 Fiber drawing machine

The fiber drawing machine consisted of a wooden rectangular frame, a fixed clamp, a movable clamp and a bolt of length 15cm (Figure 4.3). The inner front end of the machine has a shallow groove which ensures that the bolt rotates about the same axis during fiber drawing. The movable clamp is wooden with a nut firmly fixed at the centre. This nut enables the clamp to move back and forth when the bolt is rotated. A hole is drilled vertically through which another bolt, a nut and washers are fixed at the top to act as the clamp. The thread on the bolt has a pitch of length 1mm to ensure that the fiber stretches steadily during the drawing process. On the sides of the wooden box is the slide bearing which guides the movable clamp when the bolt is rotated to pull the fiber.

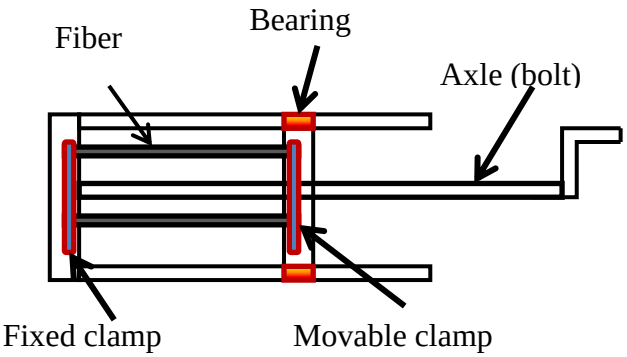

Figure 4.3: Fiber drawing machine

4.4 Sample preparation

4.4.1 Moulding PP films

Polypropylene films were prepared by using the locally made compression moulding apparatus shown in figure 4.1. The films were prepared by compression moulding of PP pellets after melting at a temperature between 165 ^{o}C and 170 ^{o}C. The mould plates were initially cleaned using steel wool and cleaning detergent. Three grams of PP pellets measured using the Shimadzu electronic balance was placed in the mould. The temperature of the mould was then raised steadily to melting point (170 - 180^{o}C). After holding the temperature constant for 150 seconds the hot plates were removed and the assembly left to air-cool for two minutes under constant pressure of 6MPa.

4.4.2 Drawing of PP fibers

Strips of length 4 to 5 cm and width 2.5 to 3mm were cut from some of the PP films. Each strip was mounted and firmly clamped in the drawing machine. Drawing was then done at room temperature (25^{o}C) by rotating the bolt at a rate of 7.2 revolutions per minute until the desired draw ratio was attained. This process was repeated several times to produce fibers of draw ratios 2, 5, 8 and 11. Draw ratios above 11 could only be achieved at temperatures above the room temperature of 25^{o}C. However, in order to maintain a consistent thermal history for all fibers 25^{o}C was used throughout the drawing process, thus limiting Dr to 11. Fibers of various draw ratios were then chopped into pieces of length 40 mm ready for composite manufacturing (Figure 4.4).

Figure 4.4: An illustration of drawn fibers

4.4.3 Fabrication of Self-reinforced polypropylene composites (SRPPCs)

Some other PP films were cut into rectangular shapes of dimensions 40mm by 25 mm by 1mm. Chopped fibers together with the rectangular films were then used to produce composites. Different sample categories were fabricated by sandwiching the fibers between two rectangular films. The hand lay-up method was used to carefully arrange the fibers to ensure even distribution. This arrangement was placed in the chamber of the composite fabrication mould (Figure 4.2) with the thermometer in place. The chamber was then firmly closed, the fabrication mould placed in the oven. The oven temperature was set to the desired consolidation temperature and heated at a rate of 5 ^{o}C per minute. A thermocouple thermometer (sensitivity ± 0.5 ^{o}C) was used to monitor the temperature rise in the specimen during heating. On attaining the desired temperature, a time dwell of 130 seconds was maintained. After the dwell time, the moulding chamber and its contents was quickly removed from the oven and subjected to a constant pressure of load of 4kg as it air-cooled before removing the composite. Shaping of the cool composite was done using a sharp blade and a file to produce a final specimen measuring 34mm by 12mm by 2.5mm. This technique of film-stacking followed by consolidation under constant load was used to produce all

the Tc sample category specimens (Tc163, Tc165, Tc167, Tc170, Tc173 and Tc175 ± 1^{o}C).

For the sample category produced by varying consolidation time (tc), consolidation temperature of 170^{o}C, fibers of draw ratio 11, and fiber weight fraction of 15 wt% were used. After raising the temperature of the chamber to 170^{o}C, specimens were held at Tc for 30, 60, 90 and 130 seconds in order to produce samples with different consolidation times (tc30, tc60, tc90, and tc130). To fabricate the sample category with draw ratio as the variable parameter, Tc = 170^{o}C, tc = 130 seconds, and fiber weight fraction of 15 wt% were used. Specimens made for this group were Dr2, Dr5, Dr8 and Dr11. The final category was the one with varying fiber weight fraction (Fw). For this sample category, Tc = 170^{o}C, tc = 130 seconds, and Dr = 11 were used to fabricate the Fw sample categories, (Fw3; specimen with fiber weight fraction 3wt%, Fw6; specimen with fiber weight fraction 6wt%, Fw9; specimen with fiber weight fraction 9wt%, Fw12; specimen with fiber weight fraction 12wt%, and Fw15; specimen with fiber weight fraction 15wt%). Fiber loading beyond 15wt% could not be achieved within the experimental conditions of this study owing to fiber packing challenges that could lead to inadequate wetting of the fibers and eventual poor fiber matrix adhesion. A summary of all parameters that were considered during fabrication of various categories of SRPPCs samples is given in table 4.1.

Table 4.1: Summary of sample categories produced and the various parameters considered

	Parameters			
Sample category	Fiber draw ratio	Consolidation temperature	Consolidation time,	Fiber weight fraction
Tc	Constant	Variable	Constant	Constant
tc	Constant	Constant	Variable	Constant
Dr	Variable	Constant	Constant	Constant
Fw	Constant	Constant	Constant	Variable
Neat	N/a	Constant	Constant	N/a

4.5 Measurements

4.5.1 Dynamic mechanical analysis of PP fiber

Dynamic mechanical analysis was performed on PP fibers of draw ratio 5, 8 and 11. Specimens were tested in a TA Instruments DMA 2980 machine operating in a tensile testing mode. The test specimen was loaded into the instrument film tension clamp and the temperature raised to 25^{o}C, allowed to stabilize for 5 minutes and then heated at a rate of 2^{o}C per minute until 120^{o}C. The frequency of oscillation was fixed at 1 Hz to minimise hysteretic heating which takes place at higher frequencies and also due to the lower thermal conductivity of the polymer matrix. At higher frequencies less time is allowed for the heat dissipation to the surroundings which can lead to temperature rise. Thermal effect due to hysteretic heating can lead to undesired deterioration of sample properties. Therefore, to ensure that only mechanical cycling leads to changes in the observed parameters, a frequency of 1 Hz was maintained. The strain amplitude was 20 μm, low enough to minimise adverse

mechanical damage to the sample under test. Storage modulus (E'), loss modulus (E'') and mechanical loss factor (tan δ) were determined during the test.

4.5.2 Dynamic mechanical analysis (DMA) of SRPP composite

DMA of self-reinforced PP composites was performed in single cantilever flexural mode. Specimens with dimensions of approximately 35mm x 12mm x 2.5mm (standard specimen dimensions for the DMA test) were tested in the DMA 2980 machine (TA Instruments) equipped with a data acquisition software. After loading the specimens the temperature was raised to 35^{o}C and allowed to stabilize. After equilibration, the chamber was heated at a rate of 2^{o}C per minute until 110^{o}C. The specimen was subjected to a sinusoidal flexural displacement applying a maximum tensile strain of 0.04 % at frequency of 1Hz. This test was carried out on all the five categories of samples prepared. The damping factor tanδ, storage and loss moduli were monitored and recorded as functions of temperature.

4.5.3 Fatigue tests

The fatigue behaviour of the SRPPCs was studied by using TA Instruments DMA 2980 machine. The DMA single frequency mode was selected. Fatigue tests were conducted in an amplitude controlled mode at a frequency of 5 Hz and stress ratio (R=1). A cyclic frequency of 5 Hz was used to prevent increase in temperature due to hysteretic heating. Such a low frequency was selected so that fatigue failure would occur instead of thermal failure. The duration of fatigue test was 140 minutes. The temperature of the experiment was kept constant at 35ºC and the specimens were

tested at 0.04% strain. Fatigue data for all the five sample categories were used to generate stiffness (storage) modulus versus number of cycles (E'–N) curves which were used to characterize fatigue behaviour of the composite.

4.5.4 Creep tests

Short-term flexural creep tests were performed using single cantilever tensile mode at different temperatures, ranging from 30^{o}C to 90^{o}C, in the DMA 2980 apparatus (TA Instruments). In this temperature range, isothermal creep tests were run on the specimens with a stepwise temperature increment of 15^{o}C. Prior to the creep measurement, each specimen was equilibrated for 5 minutes at each temperature and then the tensile creep behaviour was tested for 12 minutes, under a constant stress of 5 MPa. Specimens of dimensions approximately 18mm x 13mm x 2.5mm (length x width x thickness) were used for creep tests. This procedure was applied for all the five categories of samples prepared. The data collected was then used for analysis of creep deformation behaviour of SRPPC.

4.5.5 Thermal decomposition tests

The thermogravimetric analysis (TGA) was carried out for neat PP and SRPPCs samples using the Lindberg/blue TF55035C mini Tube furnace in oxidative atmosphere. A mass of 0.0108g of each specimen was heated from 25^{o}C at a rate of 5^{o}C per minute up to 400^{o}C, while monitoring mass change until the whole mass decomposed. Weight loss of the materials was determined and used to plot graphs of weight loss versus temperature. These results were then used to analyse the effects of consolidation temperature, consolidation time, fiber draw ratio, and fiber weight fraction on thermal properties of PP and SRPPCs.

CHAPTER FIVE

RESULTS AND DISCUSSIONS

5.1 Introduction

This chapter presents the outcomes of the experiments carried out in this study. First dynamic mechanical analysis of drawn PP fibers is discussed. Thereafter, details of the effects of consolidation time, consolidation temperature, fiber draw ratio and fiber weight fraction on dynamic mechanical properties, fatigue response, creep behaviour and thermal decomposition of SRPPCs are given. Analysis of the results using the appropriate models is also presented.

5.2 Dynamic mechanical analysis of drawn PP fibers

Figures 5.1, 5.2 and 5.3 represent the typical dynamic mechanical behaviour of PP fibers with draw ratios 5, 8, and 11 at 1 Hz in the temperature range 30 – 110^{o}C.

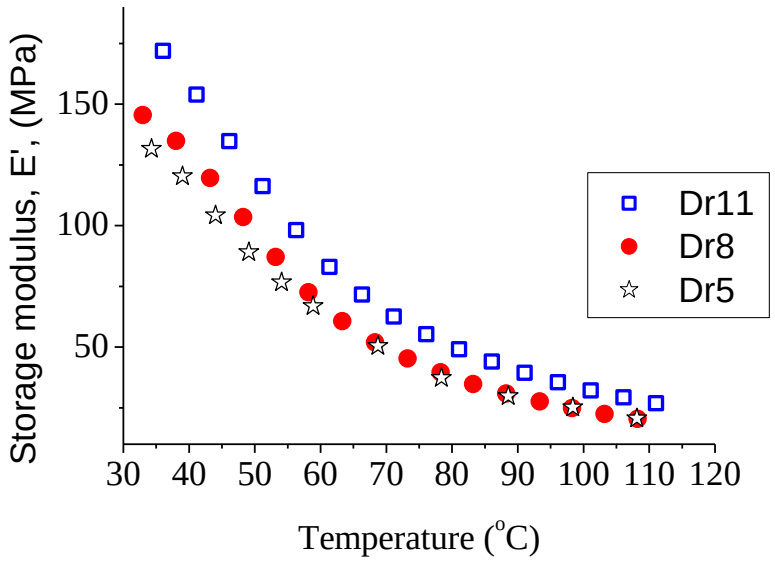

Figure 5.1: DMA plots of storage modulus versus temperature for PP fibers with draw ratios 5, 8 and 11

The graphs in figure 5.1 show that at 30 ^{o}C, the stiffness of the fibers is fairly high. Fibers with high draw ratio registered high storage modulus. Thus stiffness increased with increase in fiber draw ratio. Above 50^{o}C, the stiffness of the fibers decreases significantly. Although the fibers lost much of their elastic response above this temperature, their residual stiffness at 100^{o}C was still high (E' ≈ 13.5 MPa). High stiffness corresponding with high fiber draw ratio is attributed to the highly oriented crystals and polymer chains. This implies that the fibers possess residual orientation even at high temperature (100^{o}C). The loss modulus was also observed to increase with draw ratio. However, the effect was very minimal compared to the storage modulus. Thus, the energy dissipation property of the drawn fiber is greatly reduced (Figure 5.2).

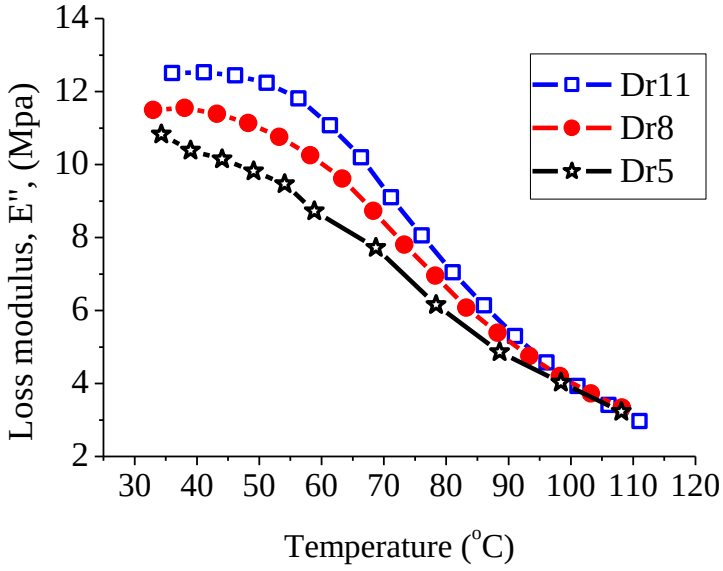

Figure 5.2: DMA plots of loss modulus versus temperature for PP fibers with draw ratios 5, 8 and 11

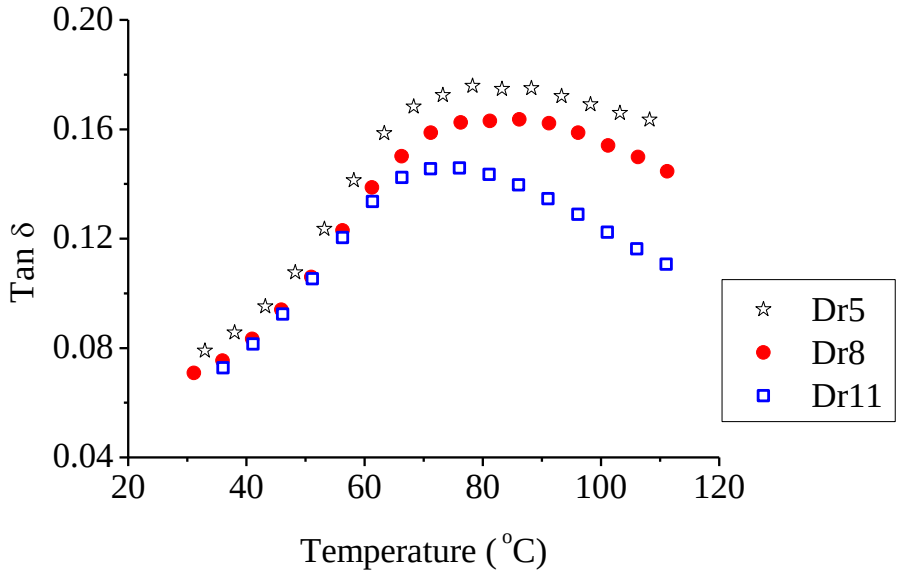

Figure 5.3: DMA plots of tan δ versus temperature for PP fibers with draw ratios 5, 8 and 11

Figure 5.3 exhibits the correlation of the tan delta with temperature which shows a maximum of 0.165 and 0.176 for fibers of draw ratios 8 and 5 respectively, at around 78°C. The loss factor for the fiber of draw ratio 11 is the lowest (0.145). Although the peak is low, the onset temperature appears to be lower, the reason being the possibility of reorientation of the amorphous chain segments aligning during the experiment. However, the decrease in the magnitude of the loss factor with draw ratio due to increased molecular interaction is maintained. Generally the tan delta peaks represent the transition temperatures (Ferry, 1970). However, figure 5.3 does not resolve any tan delta peak corresponding to the glass transition temperature of PP. The definite tan δ peak seen corresponds to the T_α transition temperature at approximately 80°C. Since these fibers are produced by drawing, it is expected that increase in drawing increases the orientation of the amorphous phase between the crystalline regions and it has less freedom to be involved in segmental motion.

Therefore, in the highly oriented PP system (Dr 11), the magnitude of the T_α peaks compared to the Dr 5 PP system is greatly reduced. The tan delta value around 80^{o}C, corresponding to α transition (Tα), is believed to be the result of molecular motions which resist the softening effect of the applied heat. While T_g reflects mobility within the amorphous regions, T_α dictates the onset of segmental motion within the crystalline regions (Boyd *et al*., 1985).

5.3 Optimisation of consolidation parameters

Dynamic mechanical analysis and creep tests were carried out on samples produced at various consolidation temperatures and consolidation times to determine the optimum consolidation conditions. Fiber draw ratio and fiber weight fraction were fixed at Dr =11 and 15 wt% respectively during the optimisation process.

5.3.1 Dynamic mechanical analysis of SRPPCs produced at different consolidation temperatures

The dynamic mechanical measurements for all the sample categories were carried out at a frequency of 1Hz, in the temperature range 30 - 125 ^{o}C, amplitude 20μm and, strain 0.04%. The results presented in this section are for samples with fiber draw ratio 11 (Dr11), fiber weight fraction of 15 wt% (Fw15), consolidation time of 130 seconds (tc130) and varied consolidation temperatures. Figures 5.4 and 5.5 show the variation of storage modulus and tan delta with temperature for specimens fabricated at consolidation temperatures 165^{o}C, 167^{o}C, 170^{o}C and, 175^{o}C. Figure 5.4 show a general decrease in the storage modulus with temperature, suggesting loss of crystallinity as temperature is increased. From the results, it can be seen that Tc170

and Tc167 have the highest storage modulus (Figure 5.4). This indicates that Tc167 and Tc170 materials are stiffer.

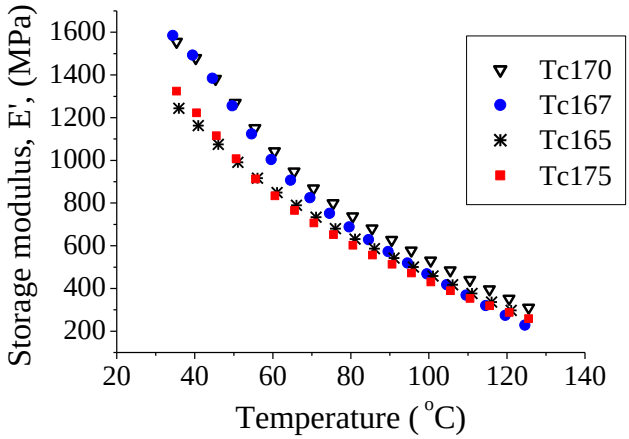

Figure 5.4: Storage modulus Versus temperature for SRPPCs produced at various consolidation temperatures

In the case of tan delta, Tc170 has the lowest magnitude of tan delta peak, indicating reduced molecular motion (Figure 5.5). Magnitudes of the peaks are highest at around 100°C for all the specimens. The peaks indicate the temperature at which large scale segmental movement of macromolecular segments occurs. Low peaks can be associated with less movement due to high interaction between the molecules leading to strong intermolecular forces resulting from excellent fiber matrix adhesion.

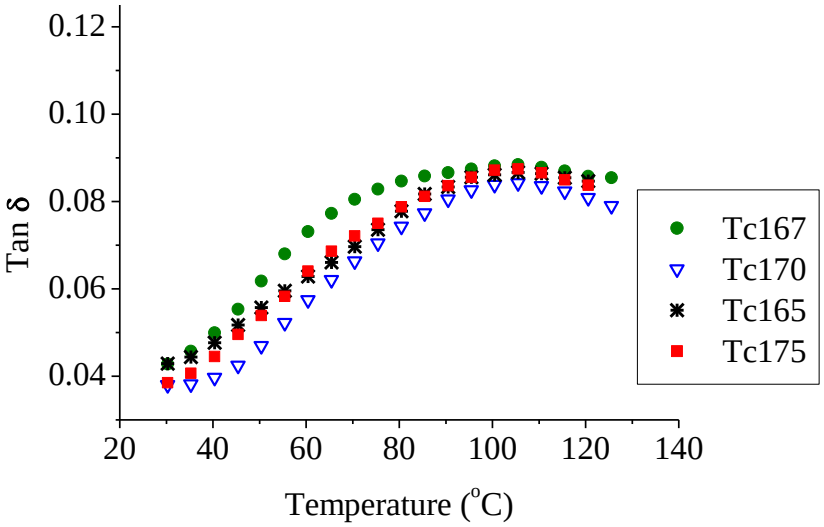

Figure 5.5: Plot of tan delta against temperature for different consolidation temperatures.

High stiffness implies good interfacial strength exhibited by the Tc170 and Tc167 is due to adequate wetting of the reinforcement by the well melted matrix. On the other hand low E' and high tan delta peaks are caused by excessive melting of the fibers that leads to loss of molecular orientation and hence destroying the crystalline structure achieved by drawing.

5.3.2 Dynamic mechanical analysis of SRPPCs produced at different consolidation times

Figures 5.6 and 5.7 depict the dynamic mechanical behaviour of SRPPCs produced at different consolidation times. Tc, Dr and Fw were held constant at 170°C, 11, and 15wt% respectively. From the results (Figure 5.6) it can be seen that storage modulus increases with consolidation time.

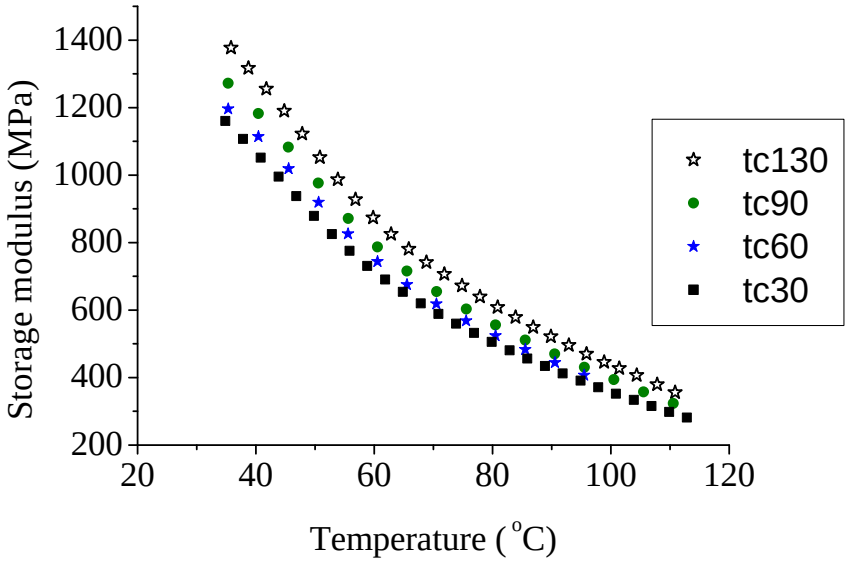

Figure 5.6: Storage modulus versus temperature for tc130, tc90, tc60 and tc 30 specimens.

This indicates that composite stiffness increases as the consolidation time is increased for the consolidation times studied. Longer time is required to ensure adequate socking of fibers by the melted matrix which enhances interfacial strength. For this sample category, the magnitudes of tan delta peaks for the specimens decrease with increasing consolidation time (Figure 5.7). Adequate time allowed for consolidation enhances the intermolecular force due to decreased inter-fiber void content hence segmental movement of chain molecules is reduced.

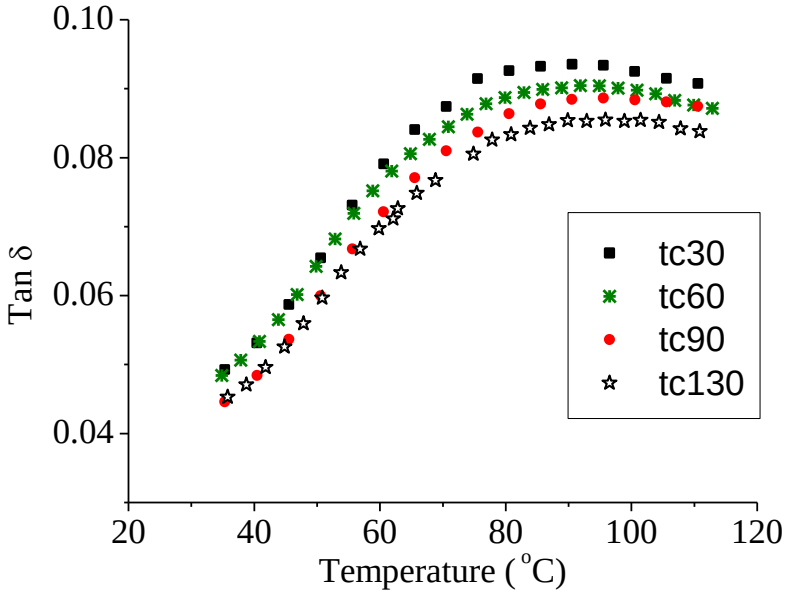

Figure 5.7: Tan δ versus temperature for tc130, tc90, tc60 and tc30 specimens.

5.3.3 Effect of consolidation temperature on creep strain of SRPPCs

The results in figure 5.8 reveal that creep strain is low for samples consolidated at 167°C and 170°C, while for consolidation temperatures below 167°C and above 170°C the creep strain increases. The results suggesting that the optimum consolidation temperature is between 167°C and 170°C.

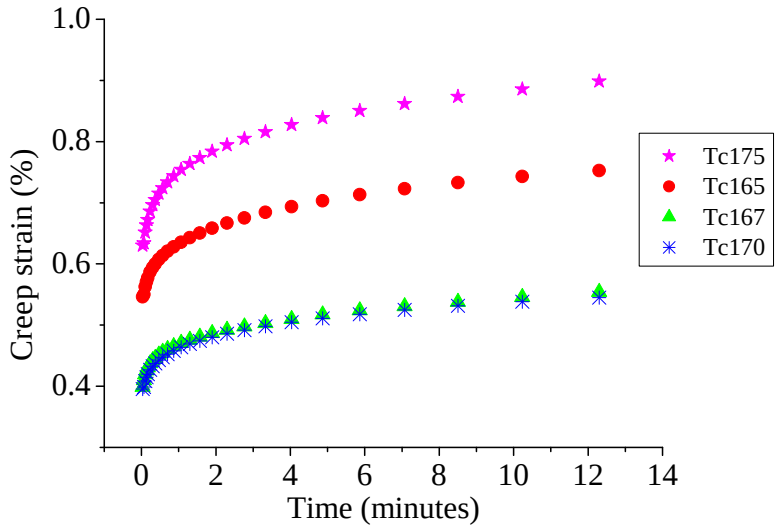

Figure 5.8: Creep strain versus time for Tc sample category

The dependence of creep deformation on consolidation temperature is explicitly illustrated by table 5.1 and figure 5.9.

Table 5.1 Creep strain values for various consolidation temperatures after creep time of 12 minutes

Consolidation temperature (^{o}C)	Creep strain (%)
163	0.85962
165	0.75237
167	0.55421
170	0.54494
173	0.79298
175	0.89866

The values used to plot figure 5.9 were obtained from figure 5.8 after creep time of 12 minutes (end of creep deformation) and are recorded in table 5.1. The shape of the plot in figure 5.9 depict that the optimum value of the consolidation temperature lies between 167^{o}C and 170^{o}C. In order to locate this value a Gaussian fit function in OriginPro7 was used, from which a value obtained of 168.6^{o}C was obtained. Low creep strain values between 167^{o}C and 170^{o}C imply that SRPPCs fabricated at these temperatures have high resistance to creep deformation, which also enhance the dimensional stability and stiffness of the material.

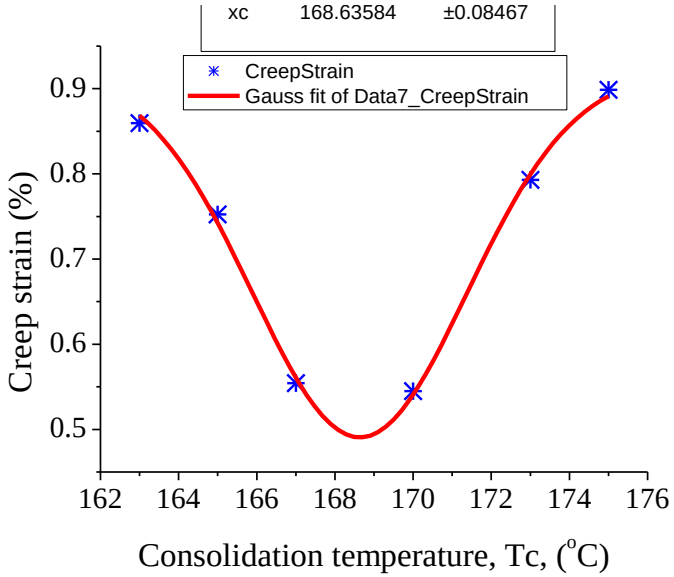

e 5.9: Variation of creep strain with consolidation temperature after creep time minutes, solid line is gaussian fit.

The creep characteristics of the SRPPC, was also analysed by considering the creep rate. This parameter represents the velocity of creep deformation and determines the dimensional stability of materials. The samples curves of creep rate (dε/dt) as a function of time are representatively given in figure 5.10. In the observed time range, the creep rate behaviour is similar in trend to creep deformation (see figure 5.10). In the primary creep stage, the creep rate started at a relatively high value and decreased rapidly with time, which might be due to orientation hardening of the material with instantaneous deformation under sudden and thereafter persistent stress. All samples exhibited high instantaneous creep at time t slightly above 0 seconds. Afterwards, differences in creep rate with respect to various consolidation temperatures became apparent. Consistent with results for creep strain, the samples produced at a consolidation temperature of 170 ^{o}C indicated the lowest creep rate.

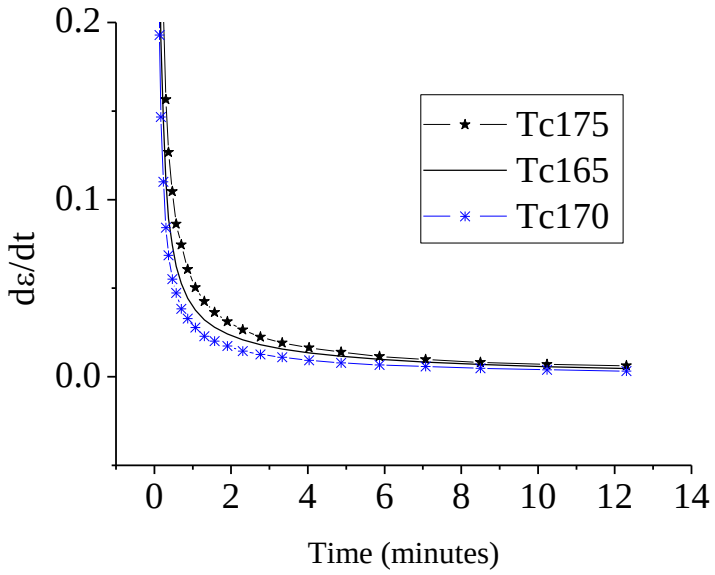

Figure 5.10: Creep rate against time for Tc sample category

The variation in creep resistance with consolidation temperature can also be attributed to the presence of inter-fiber voids which result from incomplete consolidation at temperatures below 170^{o}C. The presence of voids strongly affects the mechanical properties of the composite since the voids can make no load bearing contribution to the composite structure under stress. Low creep resistance below 170^{o}C could also be as a result of fiber/matrix debonding due to a weak interface between fibers and matrix arising from poor and incomplete wetting of the fibers by the melted matrix. Creep resistance for the fabricated SRPPC reaches a maximum when the consolidation temperature is about 170^{o}C. As the temperature is increased further, creep resistance falls due to significant melting and loss of orientation accompanied with shrinkage in the reinforcing fibers. This suggests that provided that molecular relaxation is prevented creep resistance of the composite can be maintained or even improved further. The temperature at which SRPPCs are processed influences the reinforcing effectiveness of the fibers. Very high temperatures (>Tm for fibers) is likely to melt the fibers to a large extend, whereas

very low temperatures (< Tm for fibers) are inadequate to ensure the fibers are well socked by the melted matrix to ensure good fiber/matrix adhesion.

5.3.4 Effect of consolidation time on creep of SRPPCs

Under this investigation, samples used were produced at consolidation temperature of 170^{o}C, a value that was chosen since it exhibited the lowest creep rate among the other consolidation temperature values. The fiber draw ratio and fiber weight fraction were maintained at 11 and 15 wt% respectively.

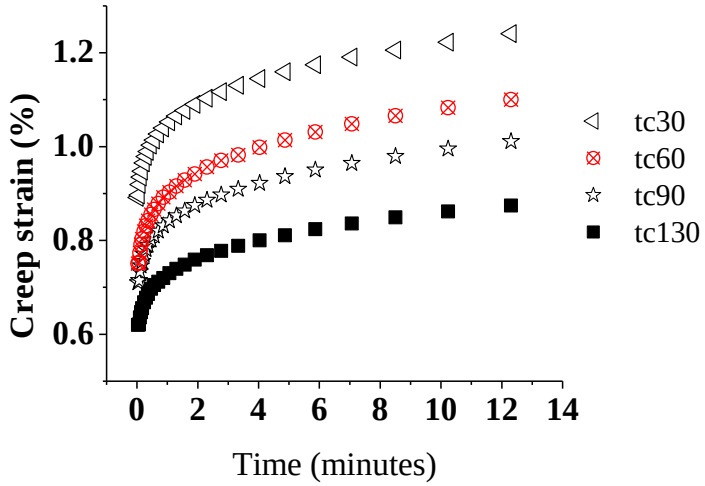

ıre 5.11: Curves of creep strain versus time for tc sample category

The creep results reported under this section include creep strain, and creep rate as functions of consolidation time during creep test. Creep strain was observed to decrease with increase in consolidation time (Figure 5.11), indicating that creep rate (Figure 5.12) was in agreement with strain.

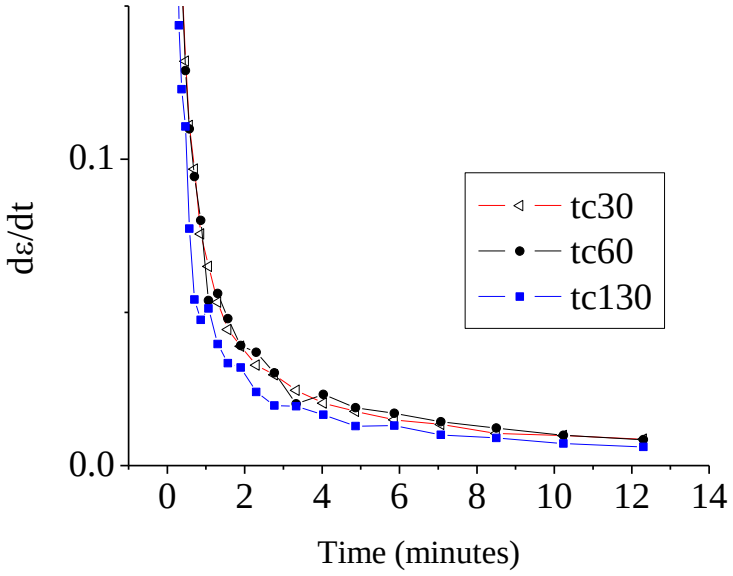

Figure 5.12: Creep rate against time for tc sample category

5.4 Effect of fiber draw ratio

5.4.1 Dynamic mechanical analysis of SRPPCs produced with PP fibers of different draw ratios

Figure 5.13 shows a plot of storage modulus E' against temperature for samples produced with fibers of draw ratios 2, 5, 8, 11 and the neat sample. The figure shows that the storage modulus E', for SRPPCs increases with fiber draw ratio at a specific temperature. Neat PP has the lowest storage modulus compared to reinforced samples. This observation emphasises the reinforcing effectiveness of the drawn PP fibers.

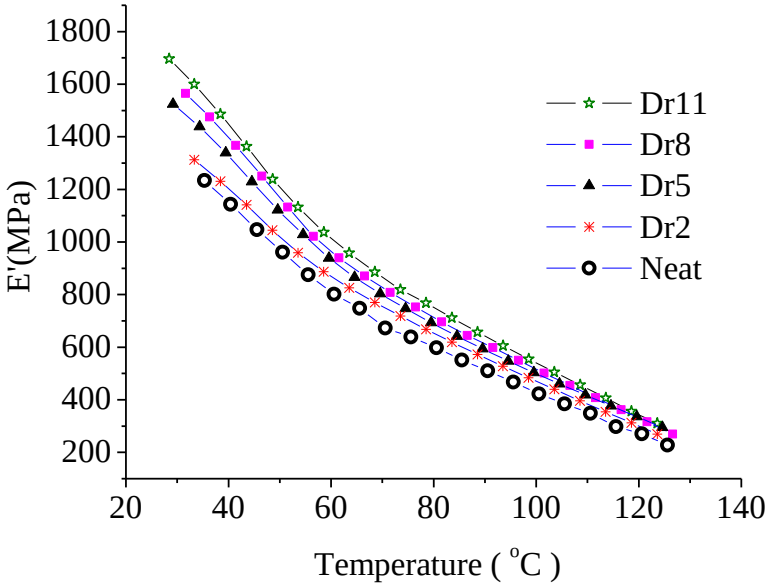

Figure 5.13: Storage modulus versus temperature for samples produced with fibers of different draw ratios

High values for E', correspond to high degree of orientation of the fibers which restricts segments of chain molecules from moving during deformation. Thus, high draw ratios cause an increase in stiffness of SRPPCs due to increased intermolecular forces. The temperature effect is as expected.

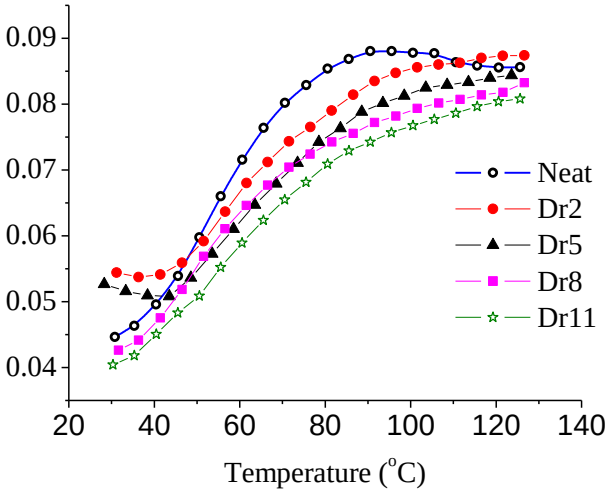

Figure 5.14: Plots of tan delta against temperature for samples produced with fibers of different draw ratios

The influence of fiber draw ratio on the loss factor (tan δ) is shown in figure 5.14. From the results, it is evident that neat PP has the highest tan delta peak with the highest magnitude (≅ 0.0881) at temperature T = 90^{o}C. The peak values for tan delta for other samples decrease gradually with increase in draw ratio. The peaks also shift to higher temperatures. The specimen with fibers of draw ratio 11 has the lowest peak at the highest temperature (tan delta ≅0.0810 at 120^{o}C).

The observed tan delta peaks above 90 ^{o}C correspond to α transition (T_{α}), and are believed to be the result of molecular motions which resist the softening effect of the applied heat. Thus, the onset of segmental motions within the crystalline regions is shifted to higher temperatures due to high orientation of the chain segments as a result of drawing. This implies that high draw ratios are preferred and hence they are highly recommended for fabrication of SRPPCs.

5.4.2 Effect of fiber draw ratio on fatigue behaviour of SRPPCs

Figures 5.15 shows the effects of different fiber draw ratios on the stiffness of the SRPPCs when subjected to cyclic fatigue. At fatigue strain amplitude of 20μm the specimen achieved 42000 stress cycles and retained high residual storage modulus with respect to the initial value at zero stress cycles. The results also show consistency with DMA results in the sense that the fatigue resistance increases with fiber draw ratio. The sample with the highest draw ratio (Dr11) registered the highest residual storage modulus due to the fact that it is stiffer, thus exhibits more elastic response.

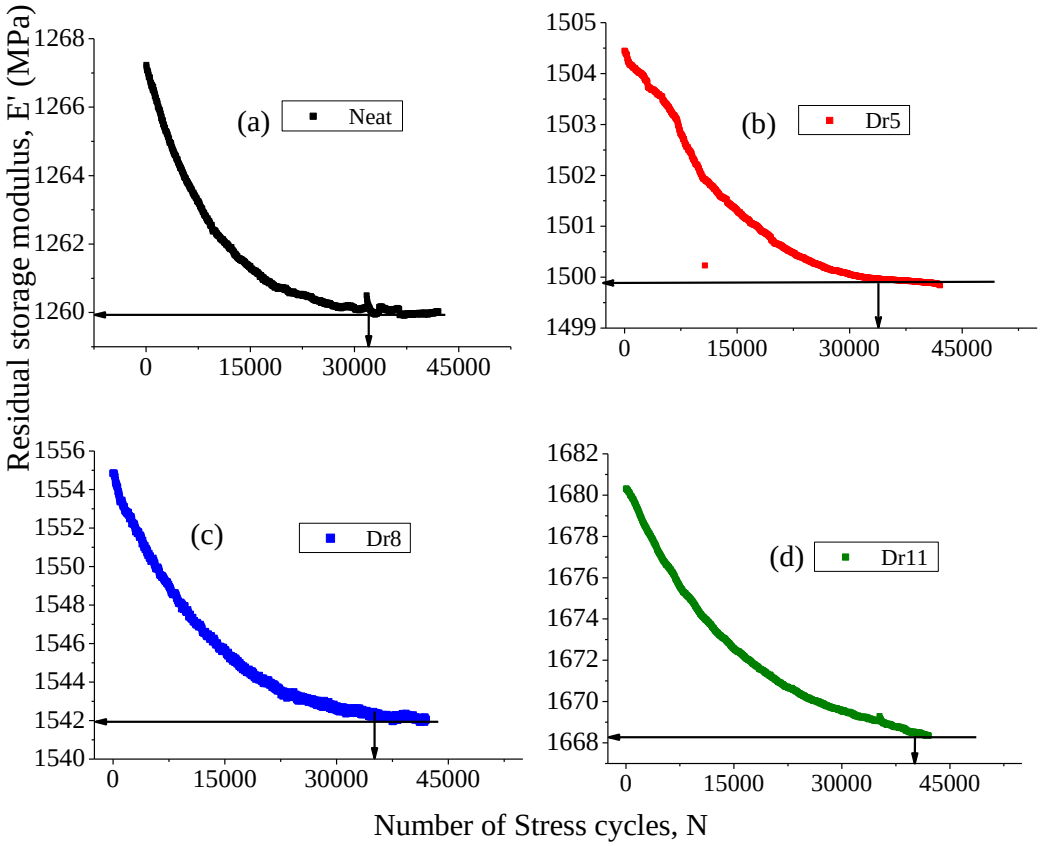

Figure 5.15: Comparison of fatigue behaviour of neat PP (a) and SRPPCs reinforced with PP fibers of draw ratios, (b) 5, (c) 8 and, (d) 11

On the other hand, the neat sample showed the lowest residual storage modulus after 42000 stress cycles compared to the reinforced specimens. This indicates that samples with lower draw ratios are more flexible. Figures 5.15 also depict the fatigue resistance and endurance limits of neat, Dr5, Dr8 and Dr11 samples. The fatigue endurance limits for the specimens were exhibited at 31900 (neat), 33800 (Dr5), and 35700 (Dr8) cycles. Specimen Dr11 registered both fatigue resistance and endurance limit of highest magnitudes (1.668GPa and 43400). This sample is stiffer, and thus exhibits more elastic response.

These results clearly indicate that, the storage moduli for all specimens decreased compared to the initial values, after fatigue life of 42000 cycles. However, these changes were small (< 0.01 GPa). In general the modulus for sample Dr11 remained high throughout the fatigue life. The composites retained high moduli values due to induced crystallinity resulting from highly oriented chain molecules that could resist segmental motions due to mechanical cycling. Also, the 5Hz frequency could not allow the chain molecules enough time to respond. Thus, high draw ratios enhance the fatigue resistance and fatigue endurance for SRPPCs. The entire specimen category exhibited a stiffness limit (E' value) below which fatigue failure would be imminent. This limit can be relied on when designing SRPPCs against fatigue failure.

5.4.3 Effect of fiber draw ratio on creep strain of SRPPCs

Samples reinforced with PP fibers of draw ratios Dr2, Dr5, Dr8 and Dr11 were subjected to a constant stress of 5MPa, for 12 minutes at a constant temperature of 35^{o}C (temperature at which materials are used in the tropical areas). Fiber weight fraction, consolidation time and consolidation temperature were kept at 15wt%, 130 seconds and 170^{o}C respectively. Consolidation pressure was maintained at 6MPa. The data obtained were used to plot curves of creep compliance against time as shown in figure 5.16. The results reveal that, creep strain decreases with increase in fiber draw ratio. Samples reinforced with fibers of draw ratio of 11 exhibited the lowest creep strain. High creep strain implies that the sample is more flexible, while low creep strain signifies resistance to creep deformation. Consequently, creep resistance was seen to increase with fiber draw ratio (Figure 5.16 (a)). Resistance to

creep is as a result of higher percentage of crystalline fraction. Drawing increases the orientation of the amorphous regions which are confined within the crystalline zones.

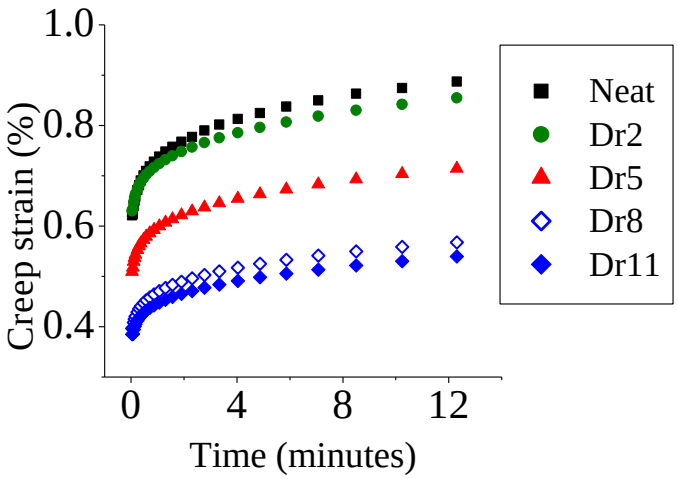

Figure 5.16 (a): Creep strain versus time for Dr sample category .

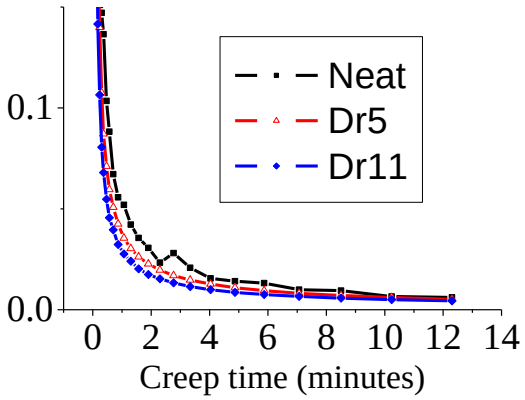

Figure 5.16 (b): Creep rate as a function of time for various draw ratios.

Thus, drawing prevents mobility of macromolecular chain segments leading to lower deformation of the composites. The drawing process stretches and straightens the polymer chain molecules. The already oriented molecules resist further stretching during creep deformation. Hence, drawing enhances creep resistance of SRPPCs.

5.4.4 Effect of fiber draw ratio on thermal decomposition of SRPPCs

Figure 5.17 shows the thermo-gravimetric analysis (TGA) results generated on SRPPCs produced with PP fibers of various draw ratios. From the graphs it can be seen that weight loss occurred in one-step degradation process from 200^{o}C to about 350^{o}C. However, the process for the neat PP was faster than for the composites. Also, the results indicate that thermal decomposition temperature increased with fiber draw ratio. Similarly, the thermal decomposition rate decreased with increase in fiber draw ratio. The changes in the decomposition mechanisms can be attributed to structural changes in the composites associated with molecular orientation due to fiber drawing.

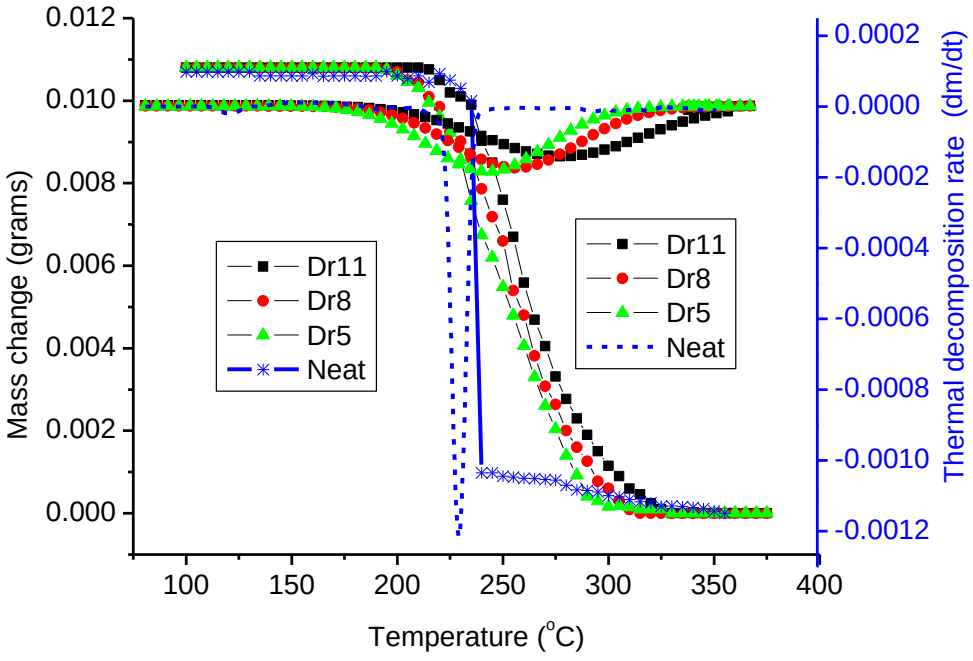

Figure 5.17: Effect of fiber draw ratio on thermal decomposition of SRPPCs

Drawing increases the crystallinity in the material as well as enhancing stiffness of the chain molecules. Consequently, the interaction between the polymer chain molecules increases. In the highly ordered state, induced by drawing, the possibility of the chains to move relative to one another is reduced as the additional forces must be overcome in the transformation to the unordered fluid state. Thus, enhanced crystallinity and stiffer molecules leads to a delay in softening and eventual melting of the composite. Hence, thermal decomposition temperature is increased and the thermal decomposition rate (a function of temperature) is lowered.

5.5 Effect of fiber weight fraction

5.5.1 Dynamic mechanical analysis of SRPPCs having different fiber weight fractions

Weight fraction (wt%) was the varied parameter during investigation of the influence of fiber weight fraction on mechanical properties. Consolidation temperature, consolidation time and fiber draw ratio were kept constant at 170^{o}C, 130 seconds and draw ratio 11 respectively. The different fiber weight fractions used were 3 wt%, 6 wt%, 9 wt%, 12 wt%, and 15 wt%.

The effect of temperature on the dynamic storage modulus and loss factor (tan delta) of the fiber weight fraction (Fw) specimens is shown in figures 5.18 and 5.19 respectively. The storage moduli of the composites clearly decreases with increasing temperature as expected in a polymer system. The moduli also increase with fiber weight fraction at a specific temperature value. The effect of fiber weight fraction on

storage modulus is more pronounced at low temperatures compared to high temperatures. High initial values of the storage modulus correspond to increased percentage of oriented fibers. A maximum value of 1806 MPa is attained as initial modulus (for Fw = 15%, figure 5.18).

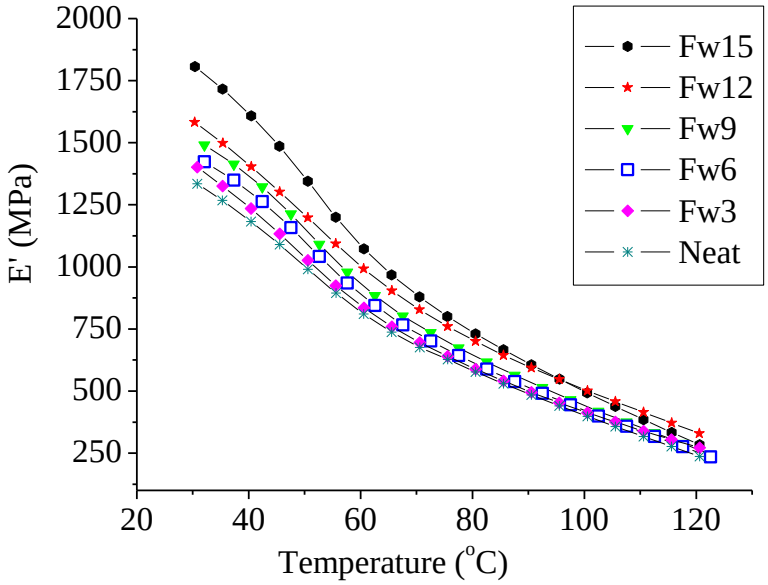

Figure 5.18: Plots of storage modulus against temperature for samples produced with different fiber weight fractions

From the graph, the curves indicate a clear trend of increasing modulus with fiber weight fraction, corresponding to increasing percentage of oriented regions. Thus, it is clear from this results that the stiffness of the composite is highly dependent on fiber weight fraction (measured by the storage modulus).

Generally the peaks of loss factor (tan delta) are associated with the glass transition temperature T_g (β relaxation) at lower temperatures and α transition temperature T_α at higher temperatures. T_g indicates mobility within the amorphous regions, whereas

T_α represents the onset of segmental motion within the crystalline regions (Reading *et al*., 1995; Acha *et al*., 2007; Hevin, 2008). PP is an "alpha mobile" polymer and therefore exhibits α transition at high temperatures.

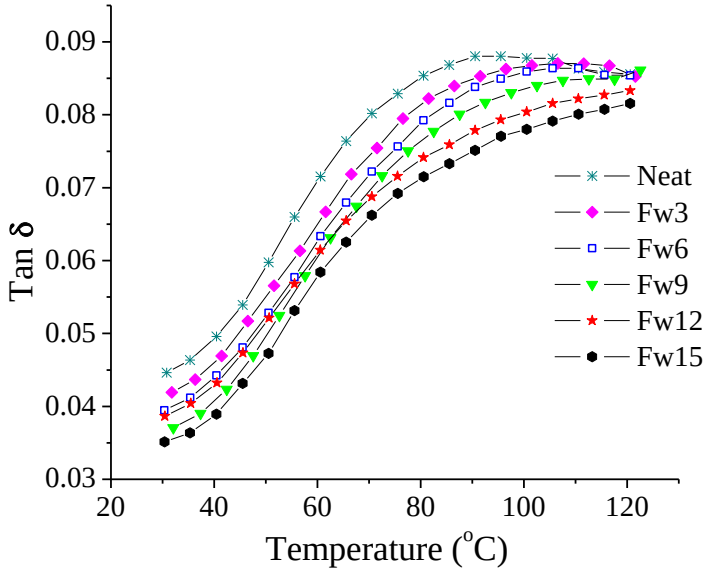

Figure 5.19: Variation of tan δ with temperature for the Fw sample category

In figure 5.19, the specimens are seen to present tan delta peaks between 85 and 125°C. It is clear that peaks for the reinforced samples are shifted towards higher temperatures and their magnitude is reduced when compared with neat PP. These observations are a result of the amorphous phase in the oriented fibers becoming highly oriented between crystalline regions (Alock *et al*., 2007). The oriented amorphous phase forms taut tie molecules, which restrict molecular segmental mobility. Therefore, the magnitude of the loss factor peaks is reduced and the temperature at which molecular motion is initiated is raised. According to figure 5.19, the tan delta peak of Fw15, although not completely developed seems to be shifted to higher temperature values by more than 25.5°C higher than that for neat PP, demonstrating the improved thermal stability of Fw15 composite. The width of

the tan delta curve for Fw15 appears to be broader signifying the high intermolecular force that resists instantaneous weakening within a narrow temperature range. Hence the sample with high fiber weight fraction is capable of withstanding a broader temperature range in applications. Thus it is clear from this results that the stiffness of the composite measured by the storage modulus is highly dependent on fiber weight fraction.

5.5.2 Effect of fiber weight fraction on fatigue behaviour of SRPPCs

The fatigue life times of samples with fiber weight fractions 3, 6, 9, and 12 are shown in figure 5.20. These results indicate that Fw15 specimen with the highest fiber weight fraction has the greatest residual modulus at the end of fatigue life (42000 cycles).

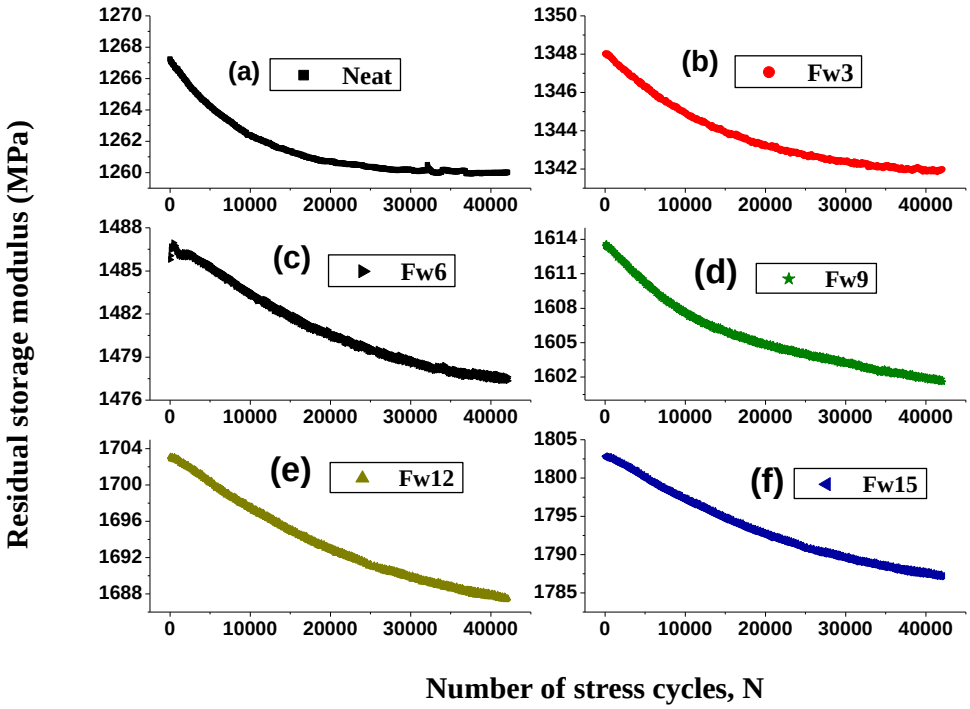

Figure 5.20: Plots of residual modulus versus number of stress cycles for samples produced with fiber weight fractions: neat (a) , Fw3 (b), Fw6 (c), Fw9 (d), Fw12 (e) and Fw15(f)

This can be attributed to the fact that samples with higher fiber weight fraction contain high crystalline structures, thus exhibiting more elastic response.

5.5.3 Effect of fiber weight fraction on creep strain of SRPPCs

The effect of PP fiber weight fraction on the creep strain of the SRPPC is shown in figure 5.21. From the results the percentage creep strain was observed to decrease with increasing fiber weight fraction. High fiber weight fraction leads to an increase in the oriented and crystalline regions which offer high resistance to polymer chain molecules segmental motion.

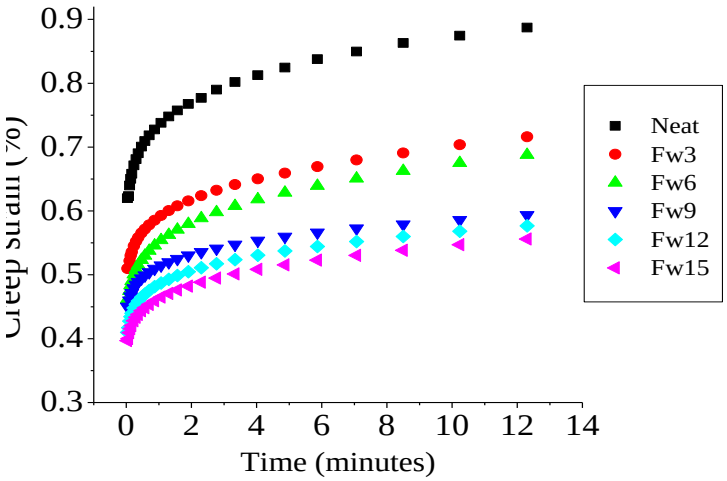

n of creep strain with time for the Fw sample category.

Table 5.3 contains creep strain values extracted from figure 5.21, at the end of 12 minutes during creep deformation. These values were plotted against fiber weight fraction as shown in figure 5.23.

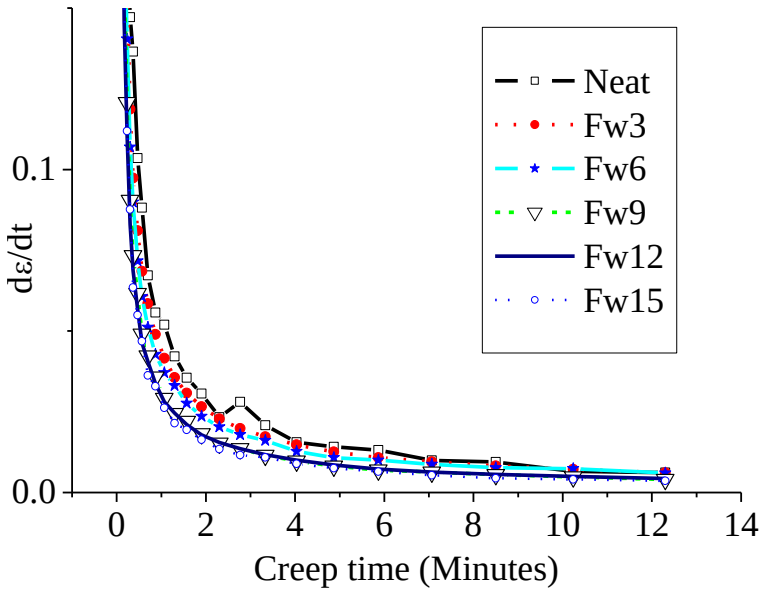

5.22: Creep rate as a function of time for the Fw sample category.

The results indicate that creep strain decreases gradually with increasing fiber loading. Thus, fiber weight fraction plays a significant role in determining the stiffness of SRPPCs.

Creep rate was also found to decrease with increase in fiber weight fraction (Figure 5.22) this can be deduced from decrease in the derivative of the creep strain with respect to creep time with increase in fiber weight fraction.

Table 5.3: Variation of creep strain with Fiber weight fraction (Fw)

Fw	Creep strain (%) at 12 minutes
0	0.88715
3	0.71619
6	0.68775
9	0.59352
12	0.57677
15	0.55612

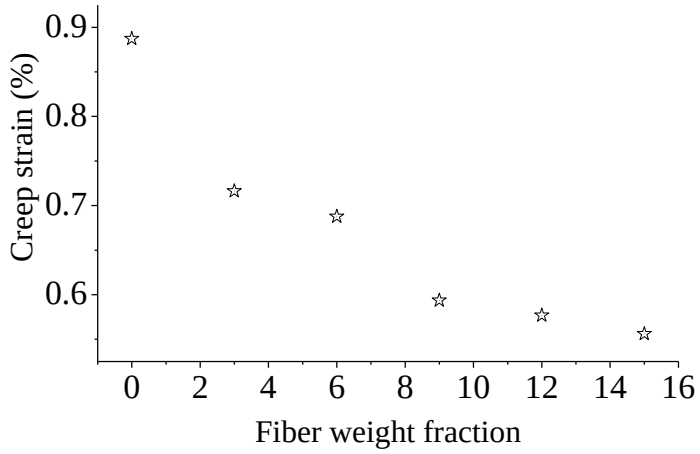

gure 5.23: Plot of creep strain versus fiber weight fraction

5.5.4 Effect of fiber weight fraction on thermal decomposition

Figure 5.24 shows the effect of fiber weight fraction on thermal decomposition of SRPPCs. It shows that thermal decomposition temperature increases with fiber weight fraction while thermal decomposition rate decreases with increasing fiber weight fraction. These can be attributed to increased crystalline structures corresponding to increase in amount of drawn fibers. The effect of the drawn fibers on the molecular structure enhances decomposition temperature and lowers thermal decomposition rate as explained under section 5.4.4. The range for the weight loss appears the same as discussed in section 5.4.4 (200 – 350 ^{o}C) with similar absolute values for mass change and thermal decomposition rate as well as the trends.

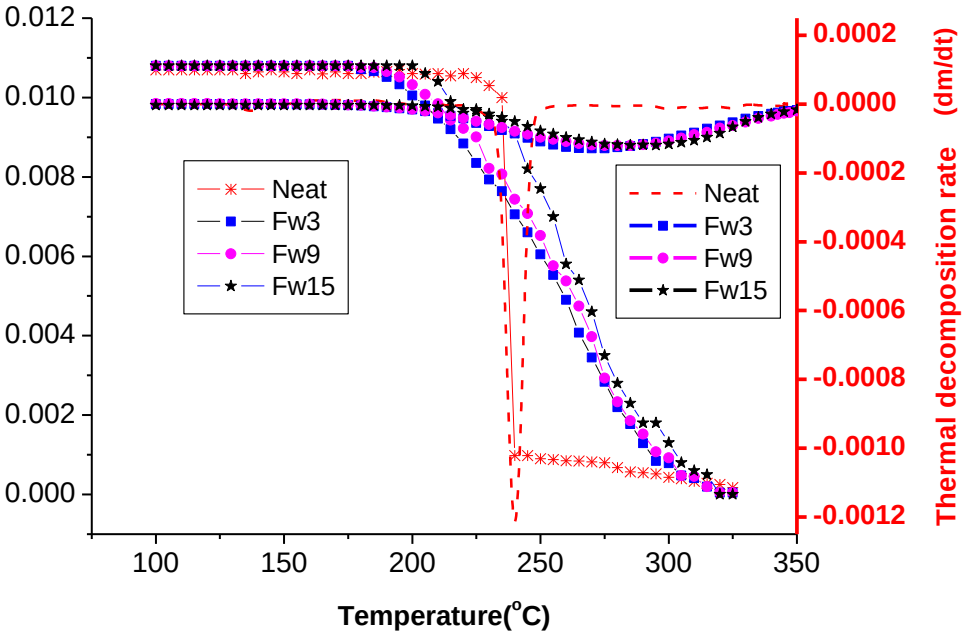

Figure 5.24: Effect of fiber weight fraction on thermal decomposition of SRPPCs

5.6 Analysis

5.6.1 Creep modelling results and analysis

5.6.1.1 Introduction

In this section creep modelling using Burgers and Findley power law models is presented. Fitting of the experimental data was done by using the Non - Linear Curve Fit function in OriginPro7. The functions of the Burger's model with four undetermined parameters and the Findley power law with three undetermined parameters were defined in OriginPro7. The initial values of the parameters were carefully chosen to make the calculation asymptotically convergent to experimental data. Otherwise the unsuitable initial values led to non-convergent result and made the fitting fail. The fitting was performed by the program using a least square approximation procedure and the parameters recorded.

5.6.1.2. Modelling parameters of Burger's model and structure-property relationship

The process of determining the initial values of the Burger's model involved first, separating the creep curve into elastic (O-A), viscous (A-B) and viscoelastic (B-C) components as illustrated in figure 5.25.

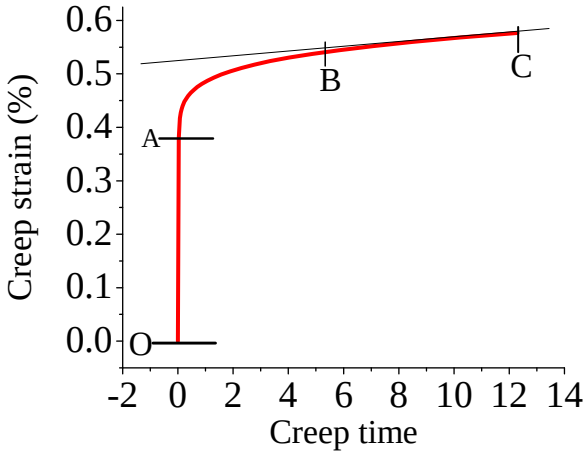

Figure 5.25: Analysis of a creep curve for Fw12wt %

The initial values for the Burger's model parameters calculated using figure 5.25 were; retardation time, τ = 0.364 minutes, modulus of the Maxwell spring, E_M = 23.16, the modulus of the Kelvin spring, E_K=15.57, viscosity of the Maxwell dashpot, η_M = 1720 and the viscosity of the Kelvin dashpot η_K = 15.

The height of section OA of the curve represents the initial instantaneous strain of the material and is equivalent to $\frac{\sigma_o}{E_M}$. From a molecular perspective this can be viewed as the elastic deformation of the polymer chains. The independent dashpots contribution, η_M, was determined by calculating the slope of the strain curve in the

region of viscous equilibrium flow BC. This equilibrium slope is equivalent to $\frac{\sigma_o}{\eta_M}$.

The curved region AB is described by the Voigt-Kelvin element of the Burger's model $\frac{\sigma_o}{E_M}\left(1-e^{-t\left(\frac{\eta_K}{E_K}\right)}\right)$ in which $\frac{\eta_K}{E_K}=\tau$ is the retardation time taken to produce 63.2% or ($1\text{-}e^{-1}$) of the total deformation of the Kelvin unit. Molecularly the dashpot in this unit can be considered to represent the resistance of the chains to uncoiling, while the spring represents vibration of chain segments that will tend to seek the lowest energy arrangement.

The representative experimental curves of creep strain versus creep time of the specimens tested at 35^o C under constant stress of 5MPa are presented in figures 5.26.

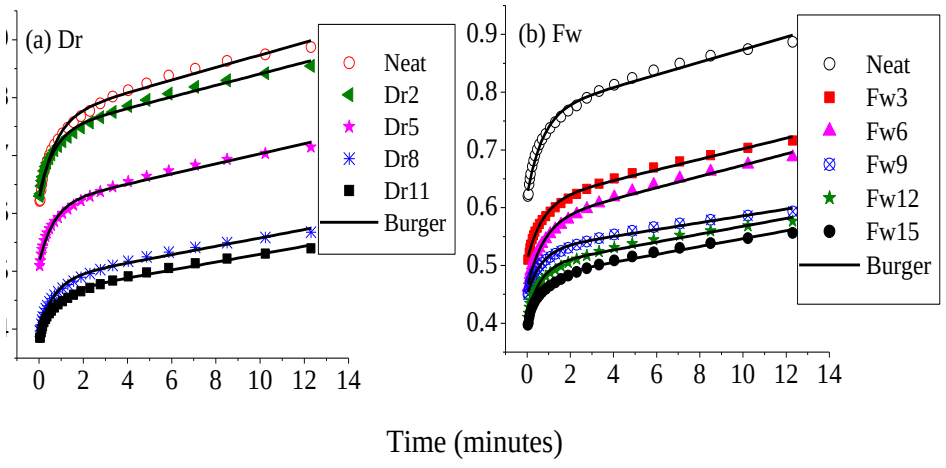

Figure 5.26: Burger modelling results of the experimental creep data obtained for samples containing various Fiber draws ratios (Dr) (a), and Fiber weight fractions (Fw) (b)

Fittings using Burgers model are drawn in black solid lines. It can be seen that the modelling curves show a satisfactory agreement with the experimental data under each condition. The first instantaneous deformation arises from the spring or elastic element (E_M) and later, time-dependent deformation comes from the parallel spring (E_K) and dashpot (η_K) and from the viscous dashpot (η_M). The complete modelling parameters for the SRPPCs are listed in table 5.4.

According to these results, all the Burger parameters showed an increasing tendency with fiber draw ratio and fiber weight fraction. The general observation is that Dr and Fw composites exhibited higher values of the parameters compared to the neat matrix. These observations strongly suggest that fiber drawing reduce molecular mobility which leads to increased stiffness and hence high resistance to deformation of the SRPPCs.

According to equation (3.19; $\varepsilon_B = \frac{\sigma_o}{E_M} + \frac{\sigma_o}{E_K}\left(1 - e^{\frac{-t\eta_K}{E_K}}\right) + \frac{\sigma_o t}{\eta_M}$), it is shown that the modulus E_M of the Maxwell spring determined the instantaneous elastic creep strain, which could be immediately recovered on the removal of stress. In general, the composites showed higher E_M values compared to the matrix (neat sample). E_M of each sample category showed an increasing tendency, which can be understood that the bulk materials become rigid and the stiffness is thus increased with the rising modulus. The instantaneous elasticity E_M reasonably corresponds to the elasticity of the crystallized polymer and oriented chains which take the immediate load due to high stiffness compared to the neat matrix. Among the observed specimens, the tc composites behaved with much lower elasticity compared to pure matrix. Better

elasticity (> 12 MPa) was exhibited by the other three categories, showing an effective reinforcement by the addition of oriented PP fibers.

Table 5.4: Parameters of the Burgers model for the SRPPCs

Sample category	Specimen	Burger parameters			
		E_M	E_K	η_M	η_K
Neat	Neat	6.15 ± 0.033	34.92 ± 1.43	460.26 ± 32.57	47.87 ± 5.76
Dr	Dr2	7.90 ± 0.045	45.86 ± 1.96	503.79 ± 30.77	66.62 ± 8.31
	Dr5	9.72 ± 0.065	49.19 ± 2.11	575.44 ± 37.27	74.25 ± 9.23
	Dr8	12.60 ± 0.08	56.29 ± 2.18	694.20 ± 43.04	81.83 ± 9.23
	Dr11	12.99 ± 0.08	65.58 ± 2.57	731.33 ± 41.87	91.42 ± 10.5
Fw	Fw3	9.81 ± 0.05	49.63 ± 1.43	547.50 ± 30.04	67.37 ± 7.50
	Fw6	10.82 ± 0.07	43.84 ± 1.71	513.45 ± 31.01	57.00 ± 6.58
	Fw9	11.13 ± 0.06	64.55 ± 2.58	847.23 ± 56.96	99.78 ± 11.48
	Fw12	12.09 ± 0.08	58.09 ± 2.39	733.06 ± 48.09	94.14 ± 11.01
	Fw15	12.54 ± 0.08	62.84 ± 2.52	735.97 ± 45.07	89.86 ± 10.53

At the molecular level, because of reduced mobility of amorphous chains and even chain folds the stiffness of the bulk material was significantly increased with high E_M.

The retardant elasticity E_K and viscosity η_K of each sample showed a similar dependency on consolidation temperature, consolidation time, fiber draw ratio and fiber weight fraction as E_M (Table 5.4). It can be described that the deformation of the Kelvin unit of the material decreased with increasing draw ratio (Dr), and fiber weight fraction Fw. The time-dependent E_K and η_K in the Kelvin unit can be associated with the stiffness and viscous or orientation flow of the amorphous polymer chains in short term. The Kelvin unit showed extremely high modulus and very difficult viscous flow, which is enhanced by good interfacial strength, reduced

void content at the optimum consolidation temperature and highly oriented fibers. It can be pointed out that fiber draw ratio and fiber weight fraction are most effective to retard the deformation of the Kelvin elements and, especially if optimum consolidation temperature is used.

The permanent viscous flow parameter η_M, which represents the irrecoverable creep, shows a factor of several tens higher than η_K (Table 5.4). It can be seen that η_M was significantly increased with high Dr and Fw, reflecting the fact of decreasing irrecoverable deformation. The irrecoverable creep strain was decreased by the addition of highly oriented PP fibers, which enhanced the immobility of polymer chains and resulted in high η_M values. Small deformation of the composite can be attributed to crystallized and oriented chains in the drawn fibers which acted as blocking sites to retard or restrict the slippage of the chain segments. The result indicates that the permanent deformation was reduced and the load applied could not activate many polymer segments or damage polymer structure permanently.

Accordingly, the bulk materials behaved with strong recoverable capability which conformed to decreased creep strain (Figures 5.16 and 5.21). Therefore, the orientation of polymer chains to a great extent resulted in highly oriented and crystallized bulk material. Thereafter, the advanced creep flow became much difficult and the resulting η_M was high.

5.6.1.3 Analysis of creep viscoelasticity by the Findley power law model

In the preceding section, the Burger's model has provided a constitutive representation of creep deformation, with the modelling parameters showing a detailed structure-to-property relationship of the self-reinforced polypropylene

composites. Findley power law is frequently applied to predict the long-term creep properties due to its simple expression and satisfactory applicability (Findley, 1989). In this research, this method was also adopted to provide a wider understanding of the creep performance of SRPPCs. The modelling curves are illustrated as solid lines in figure 5.27.

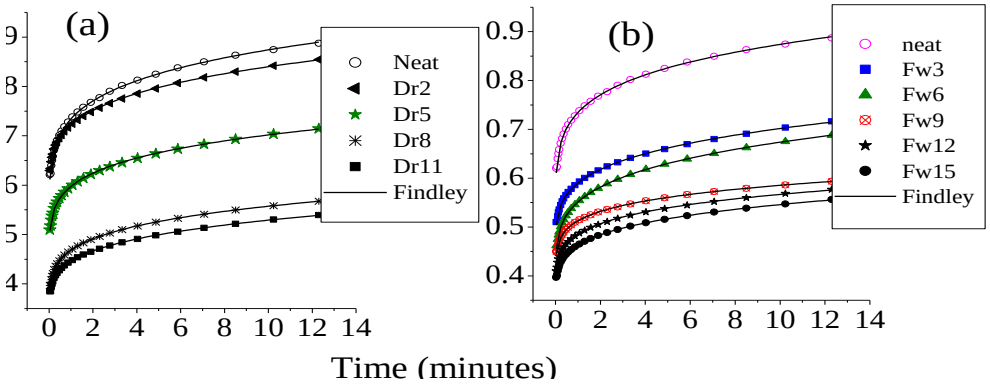

Figure 5.27: Findley modelling results of the experimental creep data obtained for samples fabricated with (a) fibers of different draw ratios, and (b) different fiber weight fractions

From the results it is evident that the fitting curves agreed very well with the experimental data. The complete modelling parameters ε_o (time-independent strain), ε_c (coefficient of time-dependent term), and n (constant independent of strain) are listed in table 5.5, from which an explicit dependency on Dr and Fw of the parameters comes into view.

Table 5.5: Parameters of the Findley power law model for the Dr and Fw sample categories compared to the neat matrix.

Sample Category	Specimens	Findley parameters		
		ε_o (%)	ε_c (%)	N
Neat	Neat	0.460 ± 0.13	0.274 ± 0.014	0.179 ± 0.009
Dr	Dr2	0.5359 ± 0.006	0.1857 ± 0.007	0.2127 ± 0.007
	Dr5	0.4060 ± 0.005	0.1918 ± 0.005	0.1883 ± 0.005
	Dr8	0.3018 ± 0.008	0.1666 ± 0.008	0.1859 ± 0.009
	Dr11	0.3206 ± 0.005	0.1255 ± 0.005	0.2207 ± 0.009
Fw	Fw3	0.4290 ± 0.006	0.1611 ± 0.007	0.2284 ± 0.009
	Fw6	0.3658 ± 0.007	0.1854 ± 0.008	0.2204 ± 0.009
	Fw9	0.3469 ± 0.011	0.1657 ± 0.011	0.1582 ± 0.010
	Fw12	0.2956 ± 0.007	0.1896 ± 0.007	0.1554 ± 0.005
	Fw15	0.3214 ± 0.005	0.1416 ± 0.005	0.2001 ± 0.007

Both the time-independent strain ε_o and time-dependent term ε_c showed apparent decrease with increasing Dr and Fw. The behaviour of ε_o was equivalent in nature to the instantaneous deformation ε_{M1} of Burger's model, while the representative parameter was the elasticity E_M of the Maxwell spring. The characteristic of ε_o was also consistent with that of E_M as discussed earlier. The values of the parameter n, varied within each sample category as well as across the sample categories indicating lack of trend. This implies that Dr and Fw do not have a strong influence on *n*.

5.6.2 Prediction of long-term properties of SRPPCs

5.6.2.1 Prediction by Time- temperature superposition principle (TTSP)

In the current investigation, short – term (12 minutes) creep experiments of SRPPCs were carried out on the Dr and Fw sample categories at five different temperatures (30, 45, 60, 75, 90^{o}C). The creep data were then shifted horizontally along the logarithmic time axis until they overlapped to form one continuous master curve, which could be used to predict creep performance over long time scale. For all the

master curves, the reference temperature was 30^{o}C. Figure 5.28 shows the creep master curves obtained. The master curves show resistance to creep by both sample categories as expected. However, the Fw15 and Dr11 samples exhibit higher intensity resistance to creep deformation. This difference in creep behaviour between the various categories can be explained by the resulting composite morphology, as discussed in the sections before, and also indicates that the characteristics of the reinforcement and the processing conditions can significantly affect the long-term viscoelastic behaviour of the self-reinforced PP composites. From the master curves, the creep behaviour of the composite could be traced over an extended time scale of order 10^8 minutes that is much wider than that determined experimentally.

Shift factors, a_T were obtained directly from the experimental creep curves plotted against time by measuring the amount of shift along the time scale necessary to superimpose the curves on the reference.

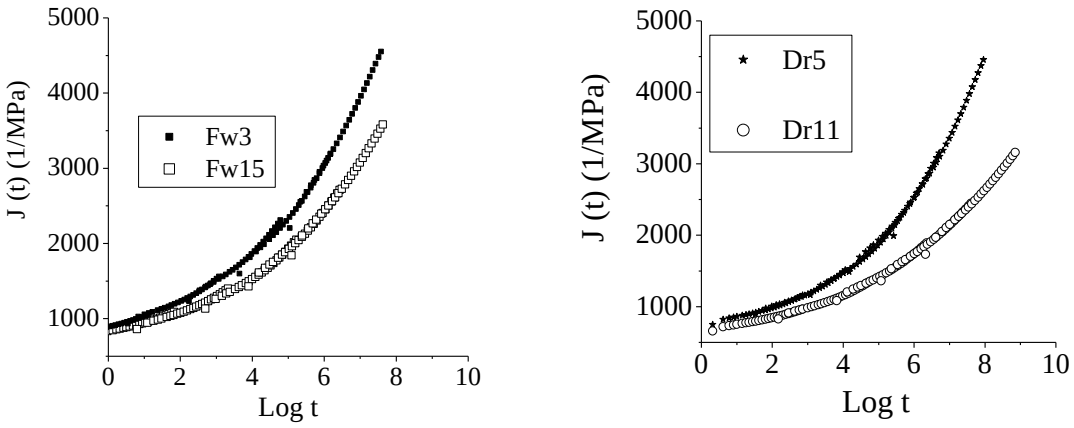

Figure 5.28: Creep master curves for various sample categories of SRPPCs

The reference temperature was taken as 30^{o}C for all the creep curves irrespective of the sample category or type. The log a_T values thus, obtained by shifting at different temperatures are listed in table 5.6. They show that the absolute value of log a_T increases with increasing temperature, it decreases with increasing fiber weight fraction and increases with fiber draw ratio. A higher shift value thus indicates a larger shift of the creep curve to the reference curve. The negative sign implies that shifting was towards the right.

Table 5.6: Shift factors (log a_T) for the SRPPCs

Temperature (^{o}C)	Log a_T			
	Fw9	Fw 15	Dr5	Dr11
30	0	0	0	0
45	-1.6	-1.3	-1.2	-1.85
60	-3.25	-3.0	-2.75	-3.5
75	-4.4	-4.15	-3.85	-4.75
90	-5.65	-5.35	-5.1	-6.0

The temperature dependence of the shift factors, a_T was also investigated using the Arrhenius relation (equation 3.24: $\log a_T = \frac{\Delta E_a}{2.303R}\left(\frac{1}{T} - \frac{1}{T_o}\right)$). When the shift factors were plotted against inverse of temperature (Figure 5.29), the resultant graphs exhibited a linear relationship. These indicate that the shift data can be best described in terms of the Arrhenius equation. The slope of each graph for the respective sample categories was calculated and used to obtain the activation energies, E_a, using the equation (3.24). The list of activation energies calculated is contained in Table 5.8. Activation energy is observed to increase with Dr, and Fw. Increase in activation energy is in agreement with increase in stiffness, creep resistance, fatigue strength and decomposition temperature. The higher activation energies also are in good

agreement with the effective reinforcing effect of drawn fibers and good fiber/matrix adhesion.

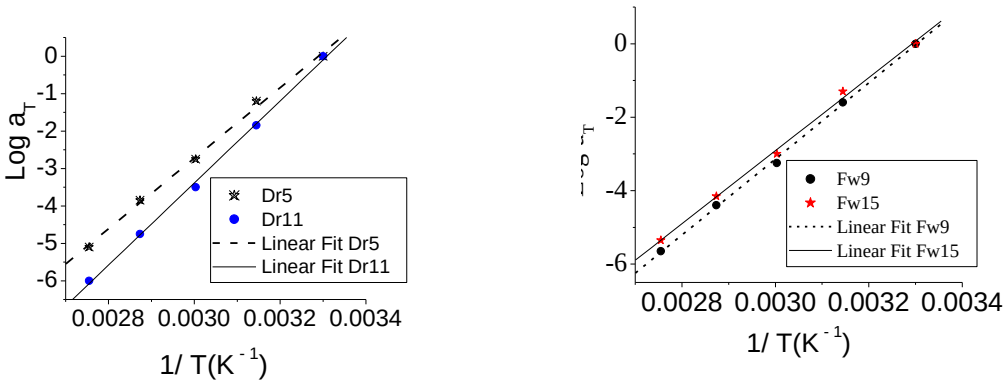

Figure 5.29: Plots of log a_T versus (1/T) for SRPPCs

Table 5.8: The activation energy for different sample categories of SRPPCs

	Fw9	Fw15	Dr5	Dr11
Slope (K)	0.093	0.129	0.114	0.127
Ea (kJ/mol)	178.1	247.0	218.3	243.2

CHAPTER SIX

CONCLUSIONS AND RECCOMENDATIONS

6.1 Conclusions

The goal of this research was to fabricate SRPPCs using PP fibers of various draw ratios and investigate the effects of consolidation temperature, consolidation time, fiber draw ratio and fiber weight fraction on dynamic mechanical properties, fatigue, and the creep behaviour of SRPPCs. Based on the results it can be seen that the consolidation conditions, fiber characteristics and fiber weight fraction determine the quality of mechanical properties of SRPPCs. Consequently the following conclusions can be made:

- During this study, it has been shown that, optimum consolidation temperature of 170^{o}C and consolidation time of 130 seconds enhances fiber/matrix adhesion.
- The composites generally showed an improvement in dynamical properties, fatigue resistance and fatigue life was significantly improved compared to the neat PP matrix. An increase of up to 33% increase in stiffness was registered over neat PP matrix.
- It was observed that stiffness, creep resistance, fatigue resistance and thermal stability improved with fiber draw ratio and fiber weight fraction. This was attributed to increased crystallinity in the drawn fibers.
- Burgers and Findley modelling parameters showed an explicit dependence on fiber characteristics. This indicated the reinforcing effectiveness of the drawn PP fibers on the SRPPCs and suggested the structure-property relationship.

6.2 Recommendations

The property improvements observed this study, makes possible the use of SRPPCs in weight sensitive applications, medical applications and applications where fatigue endurance is essential. However, the challenge remains with regard to the effect of consolidation conditions and fiber characteristics on properties other than mechanical response. Thus, further investigations on SRPPCs are proposed:

- XRD and differential scanning calorimetry (DSC) tests to quantify orientation (crystallinity) induced by drawing in relation to properties.
- Influence of drawing on other properties such energy absorption, abrasion resistance and shrinkage behaviours with the view to broaden application areas of SRPPCs.
- Influence of thermal annealing process on drawn PP fibers with a view to enhance thermal stability.
- Permeability studies on drawn fibers to investigate intra-fiber voids due to drawing.
- Carry out molecular orientation studies to investigate the improved mechanical properties of the SRPPCs.

REFERENCES

Abdullah, M.R. and Cantwell, W.J. (2005): The Impact Resistance of Polypropylene-based Fibre–Metal Laminates, *Composite Science and Technology*, **66**:1682–1693.

Abraham T. N., Siengchin S., and Karger-Kocsis J. (2008): Dynamic mechanical thermal analysis of all-PP composites based on beta and alpha polymorphic forms. *Journal of Materials Science* **43**: 3697-3703.

Acha, B., Reboredo, M., and Marcovich, E. (2007): Creep and dynamic mechanical behaviour of PP-jute composites: Effect of the interfacial adhesion. *Composites Part A-Applied Science and Manufacturing*, **38:**1507-1516.

Agarwal B., Broutman L., Chandrashekhara K.,(2006). *Analysis and Performance of Fiber Composites.* 3rd Ed., John Wiley & Sons, New Jersey.

Aifantis, E.C., (1987). The physics of plastic deformation. *International Journal of Plasticity* **3:** 211–247.

Alcock B., Cabrera N. O., Barkoula N. M., Loos J., and Peijs T. (2006): The mechanical properties of unidirectional all-polypropylene composites. *Composites Part A*: *Applied Science and Manufacturing*, **37:**716–726.

Alcock B., Cabrera N. O., Barkoula N. M., Loos J.,and Peijs T. (2007): Interfacial properties of highly oriented coextruded polypropylene tapes for the creation of recyclable all-polypropylene composites. *Journal of Applied Polymer Science*, **104**: 118-129.

Alcock B., Cabrera N. O., Barkoula N. M., Reynolds C. T., Govaert L. E., and Peijs T. (2007): The effect of temperature and strain rate on the mechanical properties of highly oriented polypropylene tapes and all-polypropylene composites. *Composites Science and Technology*, **67:** 2061-2070.

Alcock B., Cabrera N. O., Barkoula N. M., Wang Z., and Peijs T. (2008): The effect of temperature and strain rate on the impact performance of recyclable all-polypropylene composites. Composites Part B: Engineering, **39:** 537-547.

Alwis, K. G. N. C. and Burgoyne C. J., (2006): *Time-Temperature Superposition to determine the Stress-Rupture of Aramid Fibres*, Preprint, University of Cambridge, United Kingdom.

Ashbee, K. (1993). *Fundamental principles of fiber reinforced composites*. Technomic Publishing Co., Lancaster, Pa

ASTM D 2990-01, (2001): *Standard test methods for tensile, compressive, and flexural creep and creep-rupture of plastics*. West Conshohocken: ASTM International.

ASTM E 176, (1995): *"Standard Terminology of Fire Standards, "in Annual Book of ASTM standards, Vol. 4.07,* American Society For Testing and Materials, West Conshohocken, PA.

Banik K., Abraham T. N., Karger-Kocsis J. (2007): Flexural creep Behavior of unidirectional and cross-ply all-poly(propylene) (PURE (R)) composites. *Macromolecular Materials and Engineering,* **292**: 1280-1288.

Banik K., Karger-Kocsis J., Abraham T. (2008): Flexural creep of all-polypropylene composites: Model analysis. *Polymer Engineering and Science,* **48**: 941-948.

Barkoula, M., Alcock, B., Cabrera, N., and Peijs, T. (2008): Fatigue properties of highly oriented polypropylene tapes and all-polypropylene composites. *Polymer Composites,* **16:**101–113.

Bárány, T., Izer, A., and Czigány, T. (2006): On consolidation of self-reinforced polypropylene composites. *Plastic Rubber and Composites,* **35:**375–379.

Bárány, T., Karger-Kocsis, J., and Czigány, T. (2006): Development and characterization of self-reinforced poly(propylene) composites: Carded mat reinforcement. *Polymers for Advanced Technologies,* **17:** 818–824.

Bastiaansen, C. W, and Lemstra, P. J. (1989): Melting behavior of gel-spun/drawn polyolefins. *Macromolecular symposium,* **28**:73-84.

Beg M. D. H., Pickering K. L. (2008): Reprocessing of wood fibre reinforced polypropylene composites. Part I: Effects on physical and mechanical properties. *Composites Part A: Applied Science and Manufacturing,* **39:** 1091-1100.

Bhattacharyya D., Maitrot P., and Fakirov S. (2009): Polyamide 6 single polymer composites. Express Polymer Letters, **3**, 525–532.

Botev M., Betchev H., Bikiaris D., and Panayiotou C. (1999): Mechanical properties and viscoelastic behavior of basalt fiber-reinforced polypropylene. *Journal of Applied Polymer Science,* **74**, 523-531.

Bourmaud A., Baley C. (2007): Investigations on the recycling of hemp and sisal fibre reinforced polypropylene composites. *Polymer Degradation and Stability,* **92:** 1034-1045.

Bunsell A.R., Renard J., (2005). *Fundamentals of Fibre Reinforced Composite Materials*. Institute of Physics Publishing Ltd., Bristol, UK.

Cabrera, N., Alcock, B., Loos, J., and Peijs, T. (2004): Processing of all-polypropylene composites for ultimate recyclability. In: Proceedings of the institute of mechanical engineers. *Journal of Material Design and Applications,* **218:** 145–156.

Callister, Jr., W.D. (2008). *Fundamentals of materials science and engineering: an integrated approach*. Hoboken NJ: Waveland Press, Inc.

Capiati N. J., Porter R. S. (1975): Concept of one polymer composites modeled with high-density polyethylene. *Journal of Materials Science*, **10:** 1671-1677.

Chen H. B., Karger-Kocsis J., Wu J. S., and Varga J. (2010): Fracture toughness of alpha- and beta-phase polypropylene homopolymers and random- and block-copolymers. *Polymer*, **43:** 6505-6514.

Courtney, T.H. (2005): *Mechanical behavior of materials*. Long Grove, IL: Waveland Press, Inc.

Crawford, R. J., (1998): *Plastics Engineering*, Elsevier, Butterworth Heinemann, UK.

Czél G., Czigány T. (2008): A Study of Water Absorption and Mechanical Properties of Glass Fiber/Polyester Composite Pipes - Effects of Specimen Geometry and Preparation. *Journal of Composite Materials*, **42**: 2815-2827.

Czigány T., Deák T., Tamás P. (2008): Discontinuous basalt and glass fiber reinforced PP composites from textile prefabricates: Effects of interfacial modification on the mechanical performance. Composite Interfaces. **15:** 697–707.

Da Costa H. M., Ramos V. D., and de Oliveira M. G. (2007): Degradation of polypropylene (PP) during multiple extrusions: Thermal analysis, mechanical properties and analysis of variance. *Polymer Testing*, **26**: 676-684.

De Candia, F., Romano G, Victoria V, Peterlin A. (1985): Shrinkage and retractive force of drawn isotactic polypropylene during heating. *Journal of Applied Polymer science*, **30**:459-473

Deák T., Czigány T. (2009): Chemical composition and mechanical properties of basalt and glass fibers: A comparison. *Textile Research Journal*. **79:** 645–651.

Deák T., Czigány T., *Tamás., Németh Cs.*(2010): Enhancement of interfacial properties of basalt fiber reinforced nylon 6 matrix composites with silane coupling agents. *Express Polymer Letters.* **4:**590–598

DeWitt (2010): *35th Annual World Petrochemical Conference*, Houston, Texas, 24-25 March 2010; *ICB* Chemical Profile, 7 December 2010.

Directive 2000/53/EC of European Parliament and of the Council of 18 September 2000. (2000).

Echtermeyer, A.T. Engh, B., Buene L., (1995) Lifetime and Young's modulus changes of glass/phenolic and glass/ polyester composites under fatigue, *Composites,* **26** : 10-16.

Ferreira J.A.M., Costa J.D.M., Richardson M.O.W., (1996): Fatigue behaviour of a glass fibre reinforced polypropylene composite, in: *Proceedings of the 11th European Conference on Fracture*, Poitiers, France, 1653-1658.

Ferreira J.A.M., Costa J.D.M., Richardson M.O.W, (1997): Effect of notch and test conditions on the fatigue of a glass-fibre-reinforced polypropylene composite, *Composite Science and Technology,* **57:** 1243-1248.

Ferry J. D., (1980): *Viscoelastic Properties of Polymers*, 3rd Ed., John Wiley & Sons,

Fibre Glast Developments Corporation: http://www.fibreglast.com/, accessed 2/3/2014 at 10.0 pm

Findley, W.N., Lai, J.S., and Onaran, K., (1976): "*Creep and Relaxation of Nonlinear Viscoelastic Materials."* North-Holland Publishing Company, New York.

Findley, W. N., Lai, J. S., Onaran, K., (1989): *Creep and relaxation of nonlinear viscoelastic materials: with an introduction to linear viscoelasticity*. Dover Publications Inc. New York.

Flake C., Campbell, F. C, (2008): *Elements of metallurgy and engineering alloys*, ASM International, Materials Park, Ohio, USA.

Forstner R., Peters W. M., Rendina,C. J. W., Housmans, Meijer H. E. H. (2009): The influence of shear flow, cooling rate, and pressure on the specific volume of iPP and P/E random copolymers. Volumetric rheology of polymers. *Journal of Thermal Analysis and Calorimetry*, **98:**683-691

Fukui, T, Tsujii, T, Nakai, A, Hamada, H. (2002): Fabrication and mechanical properties of unidirectional PE/PE composites. *Journal of society of material science*, **51**: 1323-1328.

Fukui, T, Inoda, M, Nakai, A. Hamada, H. (2004): Fabrication and mechanical properties of textile insert injection moldings. In: *Annual technical conference of society of plastic engineers* (ANTEC), Chicago, IL, USA.

Fung, Y. C., (1972*): Stress Strain History Relations of Soft Tissues in Simple Elongation, in Biomechanics, its Foundations and Objectives*, ed. Fung, Y. C., Perrone, N. and Anliker, M., Prentice Hall, Englewood Cliffs, NJ.

Garkhail S. K., Heijenrath R. W. H., Peijs T. (2000): Mechanical properties of natural fibre-mat-reinforced thermoplastics based on flax fibres and polypropylene. *Applied Composite Materials,***7**: 351-372.

Gibson A. G. (1995): Processing and properties of reinforced polypropylenes. In 'Polypropylene: Structure, blends and composites' (eds.: J. Karger Kocsis) Chapman & Hall, London, Vol *Composites*, **71**:112.

Gilbert J. L., Lautenschlager E. P., Wright D. D. (2005): Hot compaction of poly (methyl methacrylate) composites based on fibre shrinkage results. *Journal of Material science: Materials in Medicine,* **16**:967-975.

González-González V. A., Neira-Velázquez G., Angulo-Sánchez J. L. (1998): Polypropylene chain scissions and molecular weight changes in multiple extrusion, *Polymer Degradation and Stability*, **60**: 33-42.

Hai C. T, Tinh. N, Tze-jer. C, Joannie .C, Jack, L. and Felix. H, (2000): Fatigue Model for fiber-reinforced polymeric composites. *Journal of materials in civil engineering,* **12**: 97-104.

Hamada H., Fujihara K., Harada A. (2000): The influence of sizing conditions on bending properties of continuous glass fiber reinforced polypropylene composites. *Composites Part A: Applied Science and Manufacturing*, **31**: 979-990.

Herakovich C. T. (1998). *Mechanics of Fibrous Composites*. John Wiley & Sons, New York.
Hevin P. M, (2008): *Dynamic mechanical analysis: A practical Introduction.* CRC Press, Taylor and Francis Group, Boca Raton, London New York.

Hine P. J., Ward I. M., Jordan N. D., Olley R., Bassett D. C. (2003): The hot compaction behaviour of woven oriented polypropylene fibres and tapes. I. Mechanical properties. *Polymer,* **44:** 1117-1131.

Hine P. J., Olley R. H., Ward I. M. (2008): The use of interleaved films for optimising the production and properties of hot compacted, self- reinforced polymer composites. *Composites Science and Technology*, **68**: 1413-1421.

Houshyar S., Shanks R. A. (2003): Morphology, thermal and mechanical properties of
poly(propylene) fibre-matrix composites. *Macromolecular Materials and Engineering*, **288**: 599-606.

Houshyar S., Shanks R. A. (2007): Mechanical and thermal properties of toughened polypropylene composites. *Journal of Applied Polymer Science*, **105**: 390-397.

Houshyar S., Shanks R. A. (2004): Tensile properties and creep response of polypropylene fibre composites with variation of fibre diameter. *Polymer International*, **53**: 1752-1759.

Houshyar S., Shanks R. A., Hodzic A. (2005): The effect of fiber concentration on mechanical and thermal properties of fiber-reinforced polypropylene composites. *Journal of Applied Polymer Science,* **96:** 2260-2272.

Houshyar S., Shanks R. A. (2006): Mechanical and thermal properties of flexible poly(propylene) composites. *Macromolecular Materials and Engineering,* **291**:59-67.

Houshyar S., Shanks R. A., Hodzic A. (2005): Tensile creep behaviour of polypropylene fibre reinforced polypropylene composites. *Polymer Testing*, **24**: 257-264.

Incarnato L., Scarfato P., Acierno D. (1999): Rheological and mechanical properties of recycled polypropylene. *Polymer Engineering and Science*, **39**: 749-755.

Izer A., Bárány T. (2010): Effect of consolidation on the flexural creep behaviour of allpolypropylene composite. *Express Polymer Letters*, **4**: 210-216.

Jang, B. Z, (1994): *Advanced polymer composites: Principles and applications*. ASM Internatinal, Materials Park, Ohio.

Johnson, G. A., G. A. Livesay, S. L-Y. Woo and K. R. Rajagopal, (1996). A Single Integral Finite Strain Viscoelastic Model of Ligaments and Tendons, *ASME Journal of Biomechanical Engineering*, 118**:** 221-226.

Jordan, N., Olley, R., Bassett, D., Hine, P., and Ward, I. (2002): The development of morphology during hot compaction of tensylon high modulus polyethylene tapes and woven cloths. *Polymer*, **43**: 3397–3404.

Joseph, E., Perreux, D., (1994) Fatigue behaviour of glass-fiber/ epoxy-matrix lament-wound pipes: tension loading tests and results, *Composite Science and Technology*, **52:** 469-480.

Kaplan, M. P. and, Wolff, T A, (2002): *Fatigue-Life Assessment, Failure Analysis and Prevention*, Vol.11, *ASM Handbook*, ASM International.

Karger Kocsis J. (1999): *Glass mat reinforced thermoplastic polypropylene*. In 'Polypropylene:An A-Z Reference' (eds.: J. Karger Kocsis) Kluwer Publishers, Dodrecht, **1:** 284-289.

Kitayama, T, Ishikura, K, Fukui, T, Hamada, H. (2000): Interfacial properties of PP/PP composites. *Science and Engineering of Composite Materials*, **9**:67 – 73.

Klein, N, Marom, G, Pagoretti, A, Migliaresi, C. (1995): Determining the role of interfacial transcrystallinity in composite materials by dynamic mechanical thermal analysis. *Composites*. **26**:707–712.

Kmetty, Á., Bárány, T., and Karger-Kocsis, J. (2010): Self-reinforced polymeric materials: A review. *Progress in Polymer Science*, **35**: 1288–1310.

Kwan, M. K., T. H.C., Lin, and S. L.Y. Woo, (1993): On the Viscoelastic Properties of the Anteromedial Bundle of the Anterior Cruciate Ligament, *Journal of Biomechanics*, **26**, 447-452.

Krempl, E., Khan, F., (2003): Rate (time)-dependent deformation behavior: an overview of some properties of metals and solid polymers. *International Journal of Plasticity* **19**: 1069–1095.

Lai, J. and A. Bakker, (1995): Creep and Relaxation of Nonlinear Viscoelastic Materials, *Polymer Engineering Science,* **35:**1339-1347.

Loos, J., Schimanski, T., Hofman, J., Peijs, T. and Lemstra, P.J. (2001): Morphological Investigations of Polypropylene Single-fibre Reinforced Polypropylene Model Composites, *Polymer*, **42**: 3827–3834.

Marcovich, N. E., and Villar, M. A. (2003). Thermal and mechanical characterization of linear low density polyethylene/wood flour composites. *Journal of Applied Polymer Science*, **90:**2775-2784.

Martins M. H., De Paoli M. A. (2002): Polypropylene compounding with post-consumer material: II. Reprocessing. *Polymer Degradation and Stability*, **78**: 491-495.

Matabola, K. P., DeVries, A. R., Moolman, F. S., and Luyt, A. S. (2009): Single polymer composites: A review. *Journal of Materials Science*, **44:** 6213–6222.

McCrum, N.G., Read, B.E., and Williams, G, (1991): *Anelastic and Dielectric Effects in Polymeric Solids*, Dover Publications, Inc., New York, 1991. ISBN 0-486-66752-9 (Copyright 1967 by John Wiley & Sons Ltd. and reprinted in 1991 by Dover)

Mckownm, S, and Cantwell, W.J. (2007): Investigation of Strain-rate Effects in Self-reinforced Polypropylene Composites. *Journal of Composite Materials,* **41**: 2457-2470.

Menard, K.P. (1999); "*Dynamic Mechanical Analysis: A Practical Introduction to Techniques and Applications*", CRC Press, Boca Raton

Mieck K. P. (1999): Natural fiber/polypropylene composites. in 'Polypropylene: An A-Z Reference' (eds.: J. Karger Kocsis) Kluwer Publishers, Doldrecht, *Composites*, **3**: 525-532.

Mitchel M. R, (1996): *Fundamentals of Modern Fatigue Analysis for Design, Fatigue and fracture*, vol. 19, ASM Handbook, ASM International.

Morgan, L. M., Weager, B. M., Hare, C. M., Bishop, G. R., and Smith, G. M. (2009): Self-reinforced polymer composites: Coming of age. In*'Proceeding of the 17th International Conference on Composite Materials,* Edinburgh, UK' ID, **12**:15

Morra, P.V., Morra, P.V., Radelaar, S., Yandouzi, M., Chen, J., Bottger, A.J., (2009). Precipitate coarsening-induced plasticity: low temperature creep behaviour of tempered SAE 52100. *International Journal of Plasticity* **25**: 2331–2348.

Nuriel, H, Kozlovich, N, Fieldman, Y, Marom, G. (2000). The direction properties of nylon 6,6/aramid fibre microcomposites in the presence of transcrystallinity. *Composites Part A*, **31**:69 – 78.

Park B. D, Balatinez J. J. (1998): "Short-term Flexural Creep Behavior of Wood-fiber/Polypropylene. *Composites Polymer Composites,"* **19**:377–382.

Pegoretti, A., Zanolli, A., and Migliaresi, C. (2006): Preparation and tensile mechanical properties of unidirectional liquid crystalline single polymer composites. *Composites Science and Technology,* **66**: 1970–1979.

Pegoretti A, Zanolli A, Migliaresi C. (2006): Flexural and interlaminar mechanical properties of unidirectional liquid crystalline single-polymer composites. *Composite Science and Technology*, **66:** 1953–1962.

Peijs T. (2003): Composites for recyclability. *Materials Today*, **6**: 30-35.

Peng, K., Jia, Y., Xing-Long, G. and Zhong, Z. (2011): Creep and recovery of polypropylene/carbon nanotube composites. *International Journal of Plasticity,* **10**: 1016.

Peterlin, A. (1975): Plastic deformation of polymers with fibrous structures. *Colloid polymer science*: **253**: 809-823

Philip J. D., Society of Fire Protection Engineers (SFPE) (2002*): Handbook of Fire Protection Engineering (Third Edition)*. National Fire Protection Association. Quincy, Massachusetts. USA.

Plumtree, A., and She M, G. (1991): "Fatigue damage evolution and life prediction."Proceedings, 8th International Conference on Composite Materials, 4, 38M/1-38M/10.

Pomeroy C. D. (1978): "*Creep of engineering materials."* Cambridge, U.K.
Price, D. M. (2002): "*Thermomechanical and Thermoelectrical Methods*", in P.J. Haines (ed.) Principles of Thermal Analysis & Calorimetry, Royal Society of Chemistry, Cambridge.

Ramírez-Vargas E., Navarro-Rodríguez D., Blanqueto-Menchaca A. I., Huerta-Martínez B. M., Palacios-Mezta M. (2004): Degradation effects on the rheological and mechanical properties of multi-extruded blends of impact-modified polypropylene and poly(ethylene-co-vinyl acetate). *Polymer Degradation and Stability*, **86:** 301-307.

Reading. M, and Haines. P.J, (1995); "*Thermomechanical, dynamic mechanical and associated methods" in; P. J. Haines; "Thermal methods of analysis: Principles, Applications and Problems"* Blackie, London pp.123-160.

Reed, P.H., (2003): Creep Response of FIRE and Other Burning Plasma Experiments, *Proceedings of Symposium on Fusion Engineering*, Atlantic City

Reifsnider, K. L. (1994): "Micromechanical modelling of polymeric composites. *Polymer*, **35:** 5035-5040.

Rojanapitayakorn, P., Mather, P. T., Goldberg, A. J., and Weiss, R. A. (2005): Optically transparent self-reinforced poly(ethylene terephthalate) composites: molecular orientation and mechanical properties. *Polymer*, **46**: 761–773

Rowe, G.M., M.J. Sharrock, M.G. Bouldin and R.N. Dongré, (2003): Advanced Techniques to Develop Asphalt Master Curves from the Bending Beam Rheometer, *Petroleum and Coal*, **43:**54-59.

Rust N., Ferg E. E., Masalova I. (2006): A degradation study of isotactic virgin and recycled polypropylene used in lead acid battery casings. *Polymer Testing*, **25:** 130-139.

Samuels, R. J. (1985). Polymer structure: the key to process-property control. *Polymer Engineering Science*, **25**:864-74.

Spearing. M., Beaumont, P.W.R. (1994): The fatigue mechanics of composite materials, I: experimental measurement of damage and post-fatigue properties, *Composite Science and Technology,* **44** :159-168.

Srebrenkoska V., Gaceva G. B., Avella M., Errico M. E., Gentile G. (2008): Recycling of polypropylene-based eco-composites. *Polymer International*, **57:** 1252-1257.

Stern T, Teishev A, Marom G. (1997): Composites of polyethylene reinforced with chopped polyethylene fibres: effect of transcrystalline interface, *Composite Science and Technology*. **57**:1009 – 1015.

Subramanian, S., Reifsnider, K. L., and Stinchomb, W. W. (1995): "A cumulative damage model to predict the fatigue life of composite laminates including the effect of a fiber-matrix interface."*International Journal of Fatigue*, **17:** 343-351.

Talreja, R. (1987): *Fatigue of composite materials*. Technomic Publishing Company, Lancaster, Pa.

Ţăranu N., (2009). *Composite Materials*. Course Notes. The University of Sheffield Printing
Office, UK.

Teckoe, J., Olley, R.H., Hine, P.J., and Ward, I. (1999): The morphology of woven polypropylene tapes compacted at temperatures above and below optimum. *Journal of Materials Science,* **34**: 2065-2073.

Thermal Analysis and Rheology, (2007): Application of Time-Temperature Superposition Principles to DMA, Thermal Analysis Application Brief, Number TA-144, *http://www.tainst.com (Accessed in October 2012)*.

Thomason J. L. (1999): *Mechanical and thermal properties of long glass fiber reinforced polypropylene*. in 'Polypropylene: An A-Z reference' (eds.: J. Karger Kocsis) Kluwer Publishers, Dordrecht, Vol 407-414

Thomason J. L., Vlug M. A. (1996): Influence of fibre length and concentration on the properties of glass fibre-reinforced polypropylene: 1. Tensile and flexural modulus. *Composites Part A: Applied Science and Manufacturing*, **27:** 477-484.

Thomason J. L., Groenewoud W. M. (1996): The influence of fibre length and concentration on the properties of glass fibre reinforced polypropylene: 2. Thermal properties. *Composites Part A: Applied Science and Manufacturing,* **27:** 555-565.

Thomason J. L., Vlug M. A., Schipper G., Krikor H. (1996): Influence of fibre length and concentration on the properties of glass fibre-reinforced polypropylene: 3. Strength and strain at failure. *Composites Part A: Applied Science and Manufacturing,* **27**: 1075-1084.

Thomason J. L., Vlug M. A. (1997): Influence of fibre length and concentration on the properties of glass fibre-reinforced polypropylene: 4. Impact properties. *Composites Part A: Applied Science and Manufacturing*, **28:** 277-288.

Trznadel, M, Pakula, T, Kryszewski, M. (1985): Thermally stimulated shrinkage forces in oriented polymers: 2. Time dependence. *Polymer* **26**:1011-1018.

Tschoegl, N. (1989): *The phenomenological theory of linear viscoelasticity*, Springer-Verlag, Berlin Germany.

Vaisman, L, Gonzalez, M.F, Marom, G. (2003): Transcrystallinity in brominated UHMWPE fibre reinforced HDPE composites: morphology and dielectric properties, *Polymer*, **44:**1229 –1235.

Wagner, H. Zaman, U. and Mubarak A. (2010). Physico-Mechanical Performance of Hybrid Betel Nut (Areca catechu) Short Fiber/Seaweed Polypropylene Composite, *Journal of Natural Fibers*, **7**: 165-177

Ward I. M., Hine P. J. (2004): The science and technology of hot compaction. *Polymer*, **45**: 1413-1427.

Ward I. M. (2004): Developments in oriented polymers, 1970-2004. *Plastics Rubber and Composites*, **33**: 189-194.

Ward I. M, and Hine P. J. (1997): Novel composites by hot compaction of fibers. *Polymer Engineering and Science*, **37**: 1809-1814.

Ward I. M. and Hadley D. W, (1993): *An Introduction to the Mechanical Properties of Solid*
Polymers, Wiley, New York.

Ward, I. M. (1983): *Mechanical Properties of Solid Polymers*. John Wiley and Sons Ltd., Weinheim.

William, M. L., Landel, R. F., Ferry, J. D. (1955): The temperature dependence of relaxation mechanisms in amorphous polymers and other glass-forming liquids. *Journal of America Chemical Society*, **77:**3701-3707.

Wright-Charlesworth, D., Miller, M., Miskioglu, I., and King, J. (2005): Nanoindentation of injection molded PLA and self-reinforced composite PLA after in vitro conditioning for three months. *Journal of Biomedical Material Resources Part A*, **74:**388–396.

Wu, C., (2000): Long Term Performance of Polymers, *www.me.umn.edu / divisions/ design/ composites/ Projects/ Polymer*. (accessed 18/10/2012).

Xiang Q., Xanthos M., Mitra S., Patel S. H., Guo J. (2002): Effects of melt reprocessing on volatile emissions and structural/rheological changes of unstabilized polypropylene. *Polymer Degradation and Stability*, **77:** 93-102.

Ye, L. (1989): "On fatigue damage accumulation and material degradation in composite materials. *Composite Science and Technology*, **36:** 339-350.

APPENDICES

Appendix A: Price for Chopped Strand Fiberglass Mat

Chopped Strand Mat is commonly used for build-up such as plywood decking and between layers of fabric when molding. (1.5 oz/square Feet. Mat, 38 inch and 50 inch Wide, 0.045 inch thick)

Width (inches)	**Length (Yards)**	**Price/ Roll**
38"	3 yard Roll	$27.45
38"	5 yard Roll	$38.45
50"	3 yard Roll	$32.95
50"	5 yard Roll	$49.45

(Fibre Glast Developments Corporation: http://www.fibreglast.com/)

Appendix B: Price for Fiberglass Mat Tape

1.5 oz/square feet mat, 4 inches Wide, 0.045 inches thick.

Description	**Price**
10 yard Roll	$7.65
86 yard Roll	$54.95

(Fibre Glast Developments Corporation: http://www.fibreglast.com/)

Appendix C: Price for Continuous Strand Veil Surfacing Fiberglass Mat

(38 inches wide, 0.010 inches thick)

This lightweight mat is typically used as a surfacing layer on laminations to improve surface finish and to provide a resin rich area in corrosion resistant tank linings.

Length	**Price/ Roll**
1 yard Roll	$6.55
3 yard Roll	$17.55
5 yard Roll	$21.95

(Fibre Glast Developments Corporation: http://www.fibreglast.com/)

Appendix D: Price for Continuous Strand Fiberglass Mat

(1.5 oz/square feet Mat, 50 inches wide, 0.060 inches thick)

Continuous strand mats are frequently used when rapid build-up and high conformability is required.

Length	**Price/ Roll**
1 yard Package	$12.05
3 yard Package	$27.45
5 yard Roll	$38.45

(Fibre Glast Developments Corporation: http://www.fibreglast.com/)